Indian Summer Monsoon and its relationship with ENSO as simulated by the two French CMIP5 coupled GCMs

Kamala Kakitha[1], Yannick Peings[2], Pascal Terray[1], Hervé Douville[2]

[1]LOCEAN/IPSL, CNRS/IRD/UPMC/MNHN, Paris, France
[2]CNRM, Météo-France, Toulouse, France

To be submitted to **Climate Dynamics**

16 September 2011

[1]

Corresponding author address : Pascal Terray, LOCEAN-IPSL, Université Pierre et Marie Curie, BP100 – 4 place Jussieu, 75252 Paris cedex 05, France.

Tel : +33 1 44 27 70 78

E-mail : terray@locean-ipsl.upmc.fr

Abstract

We have examined the skill of the two French state-of-the-art Coupled General ocean-atmosphere Circulation Models (CGCMs) in simulating the Indian Summer Monsoon (ISM) and its variability. For this purpose, we have considered the extensive integrations submitted to the World Climate Research Programme (WCRP) Coupled Model Intercomparison Project phase 5 (CMIP5), with ten historical coupled simulations for the Centre National de Recherches Météorologiques (CNRM) CGCM and four coupled simulations for the Institut Pierre-Simon Laplace (IPSL) CGCM both driven by natural and anthropogenic forcings. The ability of the CGCMs in simulating the seasonal mean monsoon rainfall and its relationship with El Niño-Southern Oscillation (ENSO) phenomenon at interannual and decadal timescales is studied and compared with observations and former CMIP3 simulations.

Despite improvements in the physics and/or an increase in the spatial resolution of the CGCMs, the results are not up to mark with progresses in simulating some aspects of the tropical climate variability, but also degradations of some others. In the new version of the CNRM model, the large cold SST bias found in the Tropics and Subtropics in the CMIP3 version has been largely corrected and ENSO characteristics have largely improved, but the simulation of ISM rainfall climatology is poor as compared with CMIP3 simulations. However, as a result of the significant improvements in the simulation of ENSO evolution, the CNRM model is now able to capture many aspects of the observed lead-lag relationships between ISM rainfall and El Niño events in the Pacific, but the strength of the ENSO teleconnection during boreal summer is significantly reduced compared to observations. Surprisingly, the results are opposite for the IPSL model with improvements in the ISM rainfall climatology, but a poor simulation of ENSO variability, despite of the fact that the two CGCMs share the same ocean component (but not the same sea ice model). In the case of IPSL model, the ISM rainfall climatology is far better than in previous version, but both ENSO and ENSO-ISM teleconnections have been degraded due to an incorrect phase locking of ENSO variability to the annual cycle. The amplitude of the ENSO teleconnection in the IPSL model is comparable to the observations, but the timing of this teleconnection is incorrect, peaking before the ISM onset rather than during and after ISM as observed.

Overall, these results suggest that progresses or changes in the simulation of the ISM-ENSO relationships in the two CGCMs can be traced back to modifications of ENSO characteristics in the new simulations and that the ISM rainfall climatology only plays a secondary role.

1. Introduction

The climate of South Asia is dominated by the monsoon, which returns with remarkable regularity each summer and provides the rainfall needed to sustain over 60% of the world's population. More than 80% of the annual rainfall in India is received during a short time span of four monsoon months, from June through September (JJAS hereafter). The Asian Summer Monsoon is a one of the most dominant tropical atmospheric circulation, and the economies and livelihood of the populations of India and southeast Asia depend heavily on the rainfall. Because of the dynamically interactive nature of the tropical Indo-Pacific ocean-atmosphere system and the near-global patterns of the teleconnections associated with the Indian Summer Monsoon (ISM), one of the best tools to study ISM variability is a global Coupled General Circulation Model (CGCM). In order to provide reliable seasonal predictions and climate projections of monsoon rainfall, it is nethertheless essential that CGCMs are able to produce a reasonable simulation of the mean summer monsoon circulation and rainfall distribution, as well as its variability at different time scales.

Since the pioneering work on coupled models (e.g., Manabe and Bryan, 1969; Meehl, 1995), more and more CGCMs have been developed and are currently in use worldwide (Meehl and Bony, 2011). The successive Intergovernmental Panel on Climate Change (IPCC) scientific Assessment Reports (AR) have documented the rapid growth in the skills of CGCMs, whose current versions provide state-of-the-art simulations of the present-day climate on continental and global scales (Cubasch et al., 2001; Meehl et al., 2007a). Nevertheless, this is still an area under rapid development, and CGCMs are still in a relatively early stage (Shukla et al., 2009). Furthermore, most of the models exhibit problems and deficiencies and some of them are common to many CGCMs (Mechoso et al., 1995; Dai, 2006; Lin, 2007a). As an illustration, the poor representation of rainfall in orographic regions due to coarse atmospheric resolution, the tendency to produce a double Inter Tropical Convergence Zone (ITCZ) in the Pacific and Atlantic basins, a poor representation of the annual cycle of the Sea Surface Temperature (SST) in the Tropics, particularly in the Pacific and a substantial underestimation of El Niño-Southern Oscillation (ENSO) variability are biases shared by many CGCMs in the past (Mechoso et al., 1995; Delecluse et al., 1998; AchutaRao and Sperber, 2002, 2006). Moreover, simulation of the ISM system and its variability still remains a significant challenge for many state-of-the-art CGCMs (Annamalai et al., 2007; Terray et al., 2005a, 2011; Ashrit et al. 2003).

In order to identify the reasons for these common errors, and to improve our understanding of the climate system, it is important to have a variety of different models (coupled/atmosphere-only/ocean-only), and to quantify inter-model differences. In particular, it is interesting to have CGCMs sharing some components, for example the ocean model, but differing by others (e.g. the atmospheric model) as it is the case for the two French CGCMs developed, respectively, by the Centre National de Recherches Météorologiques (CNRM) and the Institut Pierre-Simon Laplace (IPSL), and submitted to the World Climate Research Programme's (WCRP) Coupled Model Intercomparison Project phase 5 (CMIP5; Meehl and Bony, 2011). It is also important to trace back the evolution of the CGCMs and to check if the quality of the simulations has steadily improved over time with changes in the physics or resolution of the models (Meehl et al., 1997). Therefore, model evaluations have been conducted over last decades in the form of multi-model inter-comparisons. The multi-model inter-comparison has began in the late 1980s for atmospheric GCMs and continued with the Atmospheric Model Intercomparison Project (AMIP; Gates et al. 1992; Gadgil and Sajani 1998). Several other projects are now conducted specifically dedicated to CGCMs, e.g. the CLIVAR (Climate Variability and Predictability) Monsoon CGCM Intercomparison Project (Kucharski et al., 2009) and the successive phases of CMIP (Meehl et al., 2000, 2007; Covey et al 2003; Meehl and Bony, 2011).

Based upon simulation results from such state-of-the-art multi-model databases, several studies have analyzed the skill of CGCMs in simulating the mean monsoon over India and its variability. Studies focusing on the previous IPCC simulations have also noted the important distinction between changes in the monsoon circulation and rainfall anomalies (Ashrit et al., 2003; Ueda et al., 2006; Meehl et al., 2007a; Sun et al., 2010). In line with the early study by Ashrit et al. (2003), the latest IPCC AR4 indeed indicates that ISM rainfall is projected to increase due to a combination of increased moisture-holding capacity of the warmer air and the increased evaporation over the warmer Indian Ocean even while ISM circulation is likely to decrease in the future (Ueda et al., 2006; Meehl et al., 2007a; Krishna Kumar et al. 2010). Sun et al. (2010) have further analyzed the origin of the possible weakening of the monsoon circulation despite of the projected increase in near-surface land-sea thermal contrasts during the 21th century in IPCC AR4 CGCMs. Such projections must however be interpreted with caution as both the observed and simulated (by the IPCC AR4 CGCMs in the 20C3M simulations) ISM rainfall time series do not exhibit a significant (increasing/decreasing) trend over the 20th century as illustrated in Figure 1. The large spread and difficulties of the IPCC AR4 CGCMs in simulating even the mean ISM rainfall during the 20th century add further doubts about the quality of the ISM rainfall projections by the current CGCMs. Kripalani et al. (2007) have examined the climate projection over south Asia under the doubling CO2 scenario. Out of the 22 IPCC AR4 CGCMs considered, they found that only six models generate realistic 20th century monsoon climate. Climate projections using this restricted set of CGCMs reveal a significant increase in mean monsoon rainfall of 8% and a possible extension of the monsoon period. They attributed the projected increase in rainfall to the projected intensification of the heat low over northwest India, the trough of low pressure over the Indo-Gangetic plains and the land-ocean pressure gradient. Annamalai et al. (2007) have studied the monsoon-ENSO relationship in the IPCC AR4 simulations. They have also found that only six out of 18 CGCMs have a realistic representation of the present day monsoon precipitation climatology. Their study revealed that the ENSO-monsoon relationship will not weaken as the global climate warms up contrary to earlier claims (Krishna Kumar et al., 1999). The strength of the monsoon-ENSO relationship in the coupled model simulations waxes and wanes to some degree on decadal timescales, but this modulation seems intimately related to stochastic fluctuations of the climate system, which are not due to the anthropogenic signal (Gershunov et al., 2001). Furthermore, the overall magnitude and timescale for this decadal modulation is similar in the coupled model simulations and observations during the 20th century.

As a first step toward the accurate projection of monsoon rainfall, we have examined the ability of the two French CGCMs submitted to CMIP5 to simulate the ISM and its variability over the 20th century. More precisely, we have tried to document the improvements in these two models in terms of simulating the mean monsoon, its interannual variability and its relation to ENSO from CMIP3 to CMIP5. This paper is organized as follows. The models and validation datasets used in this study are described in section 2. We present the performance of the new versions of the coupled models in simulating the mean summer climate in the Indo-Pacific areas with a special emphasis on ISM and ENSO in section 3. In section 4, we analyze ISM variability and its relationship with ENSO as simulated in each model and discuss possible causes of differences in the simulation ability. The final section summarizes the main results of the present work.

2. Model and Data description

A complete and detailed description of the CMIP5 versions of the CNRM and IPSL models (CNRM-CM5 and IPSL-CM5 hereafter) can be found in reference papers in this issue, such as Voldoire et al. (this issue) and Dufresne et al. (this issue) (see also the web site http://forge.ipsl.jussieu.fr/igcmg/wiki/IPSLCMIP5 for the IPSL model) and is not repeated here. This is the lower resolution configuration of the IPSL model, which is analyzed here (Dufresne et al., 2012). The CMIP3 versions of the two models (CNRM-CM3 and IPSL-CM3 hereafter) are described in Marti et al. (2006) and Salas et al. (2005), respectively.

The main differences between the IPSL-CM3 and IPSL-CM5 are the implementation of NEMO (Madec, 2008) instead of OPA8 as oceanic component, the increase of the spatial and vertical resolutions in the atmospheric component and the inclusion of the carbon cycle in continental and oceanographic compartments of the CGCM. At CNRM, the main improvements since CMIP3 are the following. Horizontal resolution has been increased both in the atmosphere (from 2.8° to 1.4°) and the ocean (from 2° to 1°). The dynamical core of the atmospheric component has been revised. A new radiation scheme has been introduced and the treatment of tropospheric and stratospheric aerosols has been improved. The land surface scheme ISBA has been externalised from the atmospheric model through the SURFEX platform and includes new developments such as sub-grid hydrology and a new freezing scheme. The ocean model is based on the state-of-the art version of NEMO, which has greatly progressed since the OPA8.0 version used in CNRM-CM3. Finally, the coupling between the different components has also received a particular attention to ensure mass and water conservation, avoid energy loss and spurious drifts. These developments have led to a more realistic representation of the mean recent climate and to reduced drifts in a preindustrial integration (Voldoire et al., this issue).

In the present study, the focus is on historical simulations driven by both natural and anthropogenic forcings. At CNRM, a 10-member ensemble of 1850-2005 simulations has been achieved, differing only by their initial states taken at 50-yr intervals from a preindustrial run. A similar procedure has been followed at IPSL, but only a 4-member ensemble (taken at 10-yr intervals from a preindustrial run) was available at the time of writing. All simulations are forced with time-evolving historic reconstruction of observed GHGs concentrations and solar incident radiation as specified by CMIP5. The evolution of the optical depth of sulfate, organic and black carbon aerosols are taken from an LMDZ-INCA simulation forced with CMIP5 prescribed emissions in both models (Szopa *et al.*, this issue). A decadal smoothing is applied on raw data to retain the low frequency evolution of the aerosols fluctuations. Volcanic eruptions are also taken into account by prescribing the zonal mean optical thicknesses of the related stratospheric aerosols as diagnosed from Amman *et al.* (2007).

The model results have been compared with observations and re-analyses (which often in the text of this paper will also be referred to as "observations"). Specifically, we used the global analyses of Sea Surface Temperature (SST) and sea-ice HadISST (Rayner et al., 2003), the global monthly precipitation dataset from the Global Precipitation Climatology Project (GPCP), which combines measures of precipitation gauges and satellite data (Huffman et al. 2001), whereas the atmospheric fields have been compared with the European Centre for Medium-Range Weather Forecasts (ECMWF) reanalysis ERA-40 (Uppala et al. 2005). The GPCP precipitation dataset has the advantage of covering the continents and oceans, but is only available since 1979, giving a too short time record for a robust assessment of the ISM interannual to decadal variability in the CGCMs. Consequently, in discussing and validating the ISM interannual variability and the ISM-ENSO relationships, we used a land-based precipitation dataset produced by the Global Precipitation Climatology Centre (GPCC) which covers the longer period 1901-2009 (Rudolf et al., 2005).

In computing climatological means (and standard-deviations) discussed in section 3, we use the last 26 (30) yr of the CMIP5 (CMIP3) model integrations (the selected periods are, respectively, 1979-2005 and 1970-2000). Furthermore, since there are different runs (10 for CNRM-CM5 and 4 for IPSL-CM5) for the historical integrations in the CMIP5 versions of the models, we have presented the ensemble mean (and standard-deviations) of the different members for the CMIP5 results in sections 3 and 4.

In order to perform a detailed and robust evaluation of the ISM variability, both in the simulations and the observations, note that all the time series used in the analysis of section 4 have been detrended with a linear least square fit before any subsequent statistical analysis.

Here, we concentrated on the seasonal to interannual variability of ISM and its links with ENSO phenomenon (Annamalai et al. 2007, Kripalani et al. 2007, Krishna Kumar et al. 2010), longer time variations of ENSO (Wang, 1995) make such validation somewhat uncertain. However, model errors are currently larger than decadal natural variability, so that uncertainties in observations do not prevent the identification of model deficiencies in current CGCMs.

3. Boreal summer climatology and annual cycle

Modeling systems must be evaluated for their basic performance in terms of their capability to correctly reproduce the main features of the climate system. As a first step, we examine in this section the systematic errors that characterize the simulated rainfall and SST boreal summer climatologies. Annual cycles of ISM (rainfall and dynamical) indices and equatorial Pacific SSTs as simulated by the CNRM and IPSL models are also briefly discussed.

a. Coupled model simulation of boreal summer precipitation and SST climatologies

Figure 2 shows the differences between the observed and simulated rainfall and SST climatologies in order to document the evolution of the CGCMs performance from CMIP3 to CMIP5. The simulation of boreal summer precipitation climatology is proved to be a difficult task for current CGCMs and is a primary requirement that a model should possess for monsoon studies.

In the tropical Pacific, all versions of the two models are too dry over the equatorial region and tend to produce an unrealistic double rainfall ITCZ structure associated with stronger easterly trade winds over the tropical Pacific. These systematic errors are typical of many coupled models without flux adjustment (Mechoso et al., 1995; Dai, 2006; Lin, 2007a; Guilyardi et al., 2009). In all versions of the two CGCMs, there is also too much precipitation over the Maritime continent while they exhibit a dry bias over the Indian subcontinent compared to GPCP observations (excepted perhaps for CNRM-CM3). This dry bias over land is particularly evident for the IPSL-CM3 and is only partly corrected in IPSL-CM5. A lack of simulated rainfall is also visible in the eastern part of the tropical Indian Ocean (south of the equator) and over the Bay of Bengal, whereas in the western part of the Indian basin the models tend to overestimate the precipitation field.

However, from Figs. 2ab, it is evident that there is a significant reduction of the systematic errors in the tropical belt from CNRM-CM3 to CNRM-CM5 as far as the boreal summer rainfall climatology is concerned, particularly in the Pacific. Such improvements from CMIP3 to CMIP5 are not evident for the IPSL model, especially in the tropical Pacific where the double ITCZ is more prominent in IPSL-CM5 (Figs. 2cd). This is somewhat surprising taking into account that the physics in IPSL-CM3 and IPSL-CM5 are essentially the same (see section 2); these two versions differing essentially only by the latitudinal and vertical resolutions of the atmospheric model.

We now focus on the boreal summer SST climatology as simulated by the two models (Figs. 2e-h). The mean SSTs simulated by the models exhibit some substantial differences compared to the observations, both for the CMIP3 and CMIP5 versions. Starting with the CMIP3 versions, it is readily observed that, in the tropical belt, CNRM-CM3 tends in general to be much too cold, particularly along the equatorial Pacific (Fig. 2e). Overall, SSTs simulated by IPSL-CM3 are characterized by a general warm bias in the tropics with main discrepancies found at eastern boundary oceanic current areas (Fig. 2g). Superimposed over this global warm error, there is a cold tongue bias in the central and eastern equatorial Pacific associated with the double ITCZ rainfall structure and a westward extension of the easterly trade winds in IPSL-CM3 (not shown). These features suggest an overactive upwelling of cold water in the eastern and central equatorial Pacific associated with the stronger easterly trade winds via Ekman divergence as in many others coupled models without flux adjustment (Guilyardi et al., 2009). Focusing now on the CMIP5 versions of the models, the most important evolutions are the large reduction of the cold bias for the CNRM-CM5 and the substantial cooling for IPSL-CM5 in the tropical belt, but the cold tongue bias in the equatorial Pacific is still present in the current versions of the two models. Finally, the tropical warm bias in the CMIP5 versions of the models remains too strong in the upwelling regions of the three oceanic basins (during boreal summer), particularly in the southeast Pacific and to a lesser extent in the southeast Atlantic. Poor representation of coastal regions and upwelling processes in coarse ocean models and/or a lack of proper air-sea interactions, with the consequence of well-known biases in marine stratus and stratocumulus clouds, have been suggested as plausible causes for these large SST biases in the Pacific and Atlantic oceans which are recurrent and common biases to many state-of-the-art CGCMs (Lin, 2007a; Manganello and Huang, 2009).

Thus, in all versions, the models produce a too strong equatorial cold tongue which extends westward and, at the same time, tend to overestimate the SST in the south-eastern tropical Pacific giving rise to an erroneous SST gradient along the equatorial Pacific and excessive precipitation over the maritime continent. Dai (2006) suggested that the rainfall double ITCZ is related to this westward expansion of the cold tongue of SST that is observed only over the equatorial eastern Pacific, but extends to the central Pacific in the CGCMs, because models without flux corrections may have errors in heat, fresh-water and momentum exchanges. Associated positive feedbacks may amplify SST and rainfall biases and contribute also to the cold tongue and double-ITCZ problems.

b. Annual cycle of rainfall and dynamical indices over the Indian region

To asses the monsoon annual cycle in the different versions of the two GCCMs, Figure 3 displays the observed and simulated mean annual cycle of rainfall averaged over land for an Indian domain (5°N–30°N/70°E–95°E) and of the monsoon dynamical index proposed by Wang et al. (2001).

All the configurations of the models underestimate the total amount of rainfall during the ISM season (Figs. 3ab). A more detailed examination of the annual cycle of mean precipitation also reveals a significant evolution from CMIP3 to CMIP5 for the two models as far as the monsoon rainfall annual cycle is concerned. Focusing first on the IPSL model, we observe that, in IPSL-CM3, the monsoon rainfall annual cycle over the continent is very poor, to say the best, with only 2 mm/day in the months from June to September over land, (Fig. 3b) and the rainfall band is staying over the ocean (see Fig. 2c). This important systematic error has been partly corrected in IPSL-CM5 which exhibits more realistic ISM precipitation, though still with a weaker than observed amplitude (Fig. 3b). However, the ISM rainfall in IPSL-CM5 suddenly starts picking up only at the end of June, then it peaks towards the end of August (contrary to July in observations) and decreases towards the end of October (similar to observations). This problem of shifting of about one month, the monsoon seasonal cycle is also found in other CGCMs (Terray et al., 2011) and is probably related to delay in the ISM onset over the Indian subcontinent, as we will demonstrate below when discussing the annual cycle of dynamical indices of the monsoon.

The CNRM model is able to capture the annual cycle of monsoon rainfall averaged over Indian region reasonably well in both the CMIP3 and CMIP5 versions, although the timing and evolution of onset and withdraw differ slightly between the two versions (Fig. 3a). CNRM-CM5 is able to capture these two phases of the ISM much better than CNRM-CM3 when compared to the GPCC observations. Moreover, there is too much precipitation before and after the monsoon season in CNRM-CM3. However, CNRM-CM5 clearly underestimates the observed rainfall amount during the peak phase of the monsoon while the monsoon peak rainfall is reasonably simulated by CNRM-CM3.

Dynamical indices have also been developed for quantifying the seasonal cycle and interannual variability of the ISM (Webster and Yang, 1992; Wang et al., 2001). These dynamical indices can also be used to objectively assess the capability of the models in reproducing monsoon variability. One classical dynamical index has been used here: the Indian Monsoon dynamical Index (IMDI) proposed by Wang et al. (2001). The IMDI is computed as the difference in 850 hPa zonal winds averaged over 5-15°N/40-80°E and 20-30°N/70-90°E, respectively, which are the regions that undergo major shifts in wind associated with the ISM. This wind index represents the dominant mode of interannual variability in the Indian areas during boreal summer (Wang et al., 2001). Also, the large-scale monsoon and its teleconnections with other remote modes of variability such as ENSO, are expected to be well captured by these wind indices, while the rainfall over the Indian region is more closely related to regional features.

A particular strength of the CMIP5 versions of the two models is that they perform a much more realistic simulation of the annual cycle of the IMDI than their CMIP3 counterparts, with a reversal of the low-level wind shear over the North Indian Ocean from winter to summer which matches reasonably the observations (Figs. 3cd). This is somewhat surprising as far as the IPSL model is concerned since the ISM rainfall amplitude is still very weak compared to observations in the CMIP5 version (Fig. 3b). However, the IMDI annual cycle in IPSL-CM5 confirms that the onset and peak phases of ISM are delayed by one month in the current version of this model, even though the slower withdrawal phase of the monsoon is now fairly well reproduced. The simulated annual cycle of IMDI in CNRM-CM5 is in relatively good agreement with the observations in all months even if the amplitude of this simulated annual cycle is now slightly weaker than observed (Fig. 3c). However, improvements are again clearly evident from CNRM-CM3, which exhibits an IMDI amplitude much too strong during boreal summer (nearly double compared to observations) and much too weak during boreal winter.

In summary, the results presented in this paragraph stress again the importance of making a clear distinction between the dynamical and rainfall aspects of the ISM, when we will analyze CGCM's simulations in the context of the next IPCC report, since the new versions of the two CGCMs analyzed here capture reasonably well the amplitude of the Indian monsoon annual cycle from a dynamical point of view, but still show important deficiencies in terms of the rainfall annual cycle. This confirms that the ISM rainfall response cannot be inferred directly from the circulation changes over the North Indian Ocean (e.g Ashrit et al. 2003) and that, for example, fluctuations in atmospheric moisture transport play also a key role in the model's rainfall response.

c. Annual cycle of SST over the equatorial Pacific

Before presenting the interannual variability in the various configurations of the two coupled models in the next section, it is instructive to investigate how these models are able to reproduce the SST annual cycle in the equatorial Pacific because the ENSO phenomenon is strongly phased-locked to the annual cycle.

In Figure 4, we show the climatological mean annual cycle of the Niño-34 (5°S-5°N, 170°-120°W) SST from HADISST, CNRM and IPSL model simulations, respectively. The observations show a distinct asymmetric annual cycle over the Niño-34 region with the warmest (coldest) SST occurring in March–April (December–January). The Niño-34 SST annual cycle in CNRM-CM5 is entirely different from CNRM-CM3 (Fig. 4a). CNRM-CM3 is affected by a constant cold bias (-1.5 to -2°C) throughout the annual cycle and exhibits an unrealistic semi-annual cycle. Both problems are significantly alleviated in CNRM-CM5, but the coldest SSTs are still found in August-September instead of December–January. On the other hand, the Niño-34 SST annual cycle in the two versions of the IPSL model have roughly the same shape, but the current version is slightly colder in all months of about 0.5 to 1°C (Fig. 4b; this constant cold bias is corrected in the medium resolution version of the IPSL model, not shown). The main point to keep in mind is that the current versions of both the CNRM and IPSL models have a stronger than observed annual cycle in the central-eastern Pacific, with an important shift in coldest SST, both in amplitude and timing: the SST minima occurring in September in the simulations instead of December-January in observations. Moreover, in both models there is a strong cold bias of around 2°C in the month of September, already present in the CMIP3 versions.

Coupled models show a strong sensitivity to parameters tuning (Meehl et al., 2001). It is therefore difficult to know if large-scale improvements (or degradations) simulated in the tropical Pacific in the upgraded versions of the two CGCMs are due to a significant impact of changes in the physics, the resolution used or to a better (or worse) choice in the set of tuning parameters.

4. Interannual variability

a. Rainfall and SST boreal summer variability

A large fraction of the interannual variability of ISM is linked to the SST and rainfall anomalies over the Indian and Pacific oceans through atmospheric bridges (Wang, 2006). Hence, better representation of global rainfall and SST variability in the coupled models are also very important for simulating ISM variability realistically. Figure 5 shows the differences between the mean boreal summer (JJAS) precipitation and SST standard-deviations as simulated by the different versions of the two models and observations.

CNRM-CM3 produces excessive SST variability all along the equatorial Pacific (but with two particularly important nodes, in the western and eastern equatorial Pacific), and to a lesser extent in the western Indian Ocean, the North Pacific and the tropical Atlantic, e.g. in regions which are known to be largely affected by ENSO through fast atmospheric teleconnections (Alexander et al., 2002). This suggests that the simulated ENSO variability extends too far west and is exaggerated compared to the observations in CNRM-CM3 (Fig. 5e). The monthly standard-deviations of the Niño-3.4 SST is in excess of 1 to 1.5 °C during nearly all months in CNRM-CM3 as compared to observed data (see Figure 7 below). This is in contrast with most other IPCC AR4 coupled models without flux adjustment which exhibit reduced Niño-3.4 SST interannual variability (Achutarao and Sperber, 2006). Consistently, the biases in rainfall variability have also a longitudinal distribution in the tropical Pacific, but with excessive variability in the west and reduced variability in the eastern equatorial Pacific (Fig. 5a). These problems are probably linked to the cold tongue bias and associated atmospheric errors affecting CNRM-CM3 as described in section 3. Moreover, this exaggerated and mislocated ENSO mode leads to disastrous model errors in the ISM-ENSO relationships, as we will illustrate below. However, it is noteworthy, that all the above systematic errors affecting the precipitation and SST variability have been successfully reduced in CNRM-CM5 (Figs. 5bf). In this respect, the evolution of the CNRM model from CMIP3 to CMIP5 is quite impressive.

On the other hand, the systematic errors concerning the boreal summer precipitation and SST variability in the two versions of the IPSL model have nearly the same geographical distributions (Figs. 5cd and 5gh). This is consistent with the fact that the physics are exactly the same in the two versions. However, the amplitude of both the rainfall and SST variability's biases has increased in the tropical Pacific, which is an unexpected feature, probably in relation with the increased spatial and vertical resolutions in IPSL-CM5 and the related tuning of the model (see section 2). Moreover, the systematic errors concerning the rainfall variability in the tropical Pacific have a clear symmetric distribution with respect to the equator, which is reminiscent of the double ITCZ and cold tongue problems affecting the Pacific mean state in IPSL-CM5.

b. ENSO variability

Though considerable improvements in the simulation of ENSO have been made during the past twenty years, current coupled models still need to be improved with regard to realistically representing ENSO (Guilyardi et al., 2009). Here, the ENSO characteristics simulated by the two coupled GCMs and improvements made from CMIP3 to CMIP5 will be evaluated in more details.

The observed ENSO is a broadband phenomenon with a wide spectral peak between period 3–6 years. This feature has been often validated in models by examining the power spectrum of the Niño-3.4 SSTs (Achutarao and Sperber, 2002, 2006). In Figure 6, we show the Niño-3.4 SSTs power spectrum estimated from the observations (HADISST) and all the CMIP5 to CMIP3 historical simulations available from the two coupled models. The spectral density is estimated for the period 1900-2000, after removal of the seasonal cycle and linear trend for both the HadISST1.1 dataset or the simulations, by using a “classic” Fast Fourier Transform algorithm on overlapping segments (Welch, 1967). Thus, computations are exactly similar for the experiments and the observations. Note, finally, that the dashed curves in Fig. 6 show the point-wise 99% confidence limits for the Niño-34 SST spectrum estimated from the observations. These confidence limits will be used to assess how realistic are the different spectra estimated from the simulations. For additional technical details on spectral analysis, the reader is referred to von Storch and Zwiers (1999). As expected, observed Niño-34 SSTs display a broad peak from 3 to 5 yr, but is also affected by decadal variability (An and Wang, 2000). The Niño-34 SST spectra in the CMIP3 versions of the two models fall above the point-wise 99% confidence limits computed from the observed spectrum in the interannual range and are thus not realistic (Figs. 6ab). The power on quasi-triennial (i.e. between 3 and 4 years) and quasi-biennial (i.e. around 2 years) time scales is significantly enhanced for, respectively, the CNRM-CM3 and IPSL-CM3 spectral densities compared to the observations. This suggests that ENSO is too regular, with a too short periodicity of 30-50 and 20-40 months for, respectively, the CNRM-CM3 and IPSL-CM3. Interestingly, the CMIP5 versions of the models perform much better in their representation of ENSO frequency. The spectral peak in CNRM-CM5 still falls above the point-wise 99% confidence limits computed from the observed spectrum, but the magnitude of this spectral peak is largely reduced compared to the one in the CMIP3 spectrum (Fig. 6a). This suggests that the simulated ENSO mode in CNRM-CM5 is still too regular with improper representation of the pre-El Niño (before the onset of warm/cold events) atmospheric and SST patterns (see below). The IPSL model has now a much weakest peak in the Niño-34 SSTs spectrum and the shape of the spectrum now matches roughly the observed spectrum for all periods greater than one year, despite some significant loss of power around 50-60 months (Fig. 6b). Furthermore, IPSL-CM5 spectral density estimates remain within the 99% confidence interval derived from the observations for periods ranging from annual to interannual time-scales. This is a distinctive advantage of the IPSL model compared to other state-of-the-art CGCMs as far as ENSO is concerned (AchutaRao and Sperber, 2006). Another remarkable property of both CNRM and IPSL models is that the spectral characteristics of ENSO are somewhat stable across the different members of the historical simulations in CMIP5. This is in contrast to other CGCMs such as the GFDL model, which exhibits a large internal low-frequency modulation of ENSO variability and frequency at least in preindustrial integrations (Lin, 2007b; Wittenberg, 2009).

The apparent phase locking of ENSO events to the mean annual cycle with a tendency to peak at the end of the calendar year is perhaps one of ENSO's most distinctive characteristics (Rasmusson and Carpenter, 1983). In Figure 7, we show the monthly standard deviations of the Niño-34 SST anomalies from the observations and the two models, for both their CMIP3 and CMIP5 versions. Observed ENSO variability typically peaks in boreal winter and diminishes in boreal spring with relatively weak variability in boreal summer and early fall (Fig. 7). This is partly explained by the fact that the onset of El Niño events frequently occurs in boreal spring. It is apparent that the CNRM coupled model is correctly phase-locked to the annual cycle and has a preference for relatively high SST variability in the Niño-34 region during the winter season, as observed (Fig. 7a). However, the standard deviations in the CNRM-CM3 simulations are much higher than observed, suggesting again an exaggerated ENSO variability, but this bias has been eliminated in CNRM-CM5. The situation is, however, radically different for the IPSL model (Fig. 7b). The CMIP3 version has a reasonable phase locking of Niño-34 SST variability to the annual cycle, though with a weaker than observed variability during boreal winter. However, this feature has been completely destroyed in IPSL-CM5 in which the Niño-34 SST variability is higher during May to July and much less in the remaining months. This feature is due to the erroneous SST and rainfall annual cycles found in the central to eastern tropical Pacific in the current version of the IPSL model (not shown). As we will illustrate later, this bias is particularly detrimental to the simulation of the ISM-ENSO lead-lag relationships in the IPSL model.

In order to illustrate that both models have also problems in the simulation of the space-time evolution of SST anomalies associated with ENSO, we show the correlations of the DJF Niño-34 SST time series with bi-monthly Indo-Pacific SSTs in Figure 8. For the sake of brevity, we only show the results for the CMIP5 versions and observations. The too periodic nature of ENSO in the CNRM model is manifested by the existence of significant negative correlations in the eastern Pacific during the late boreal winter and spring (from February to May) before ENSO's onset, which are not seen in the observations (Figs. 8ab). The observed patterns from the onset to the peak of ENSO events show the emergence of a broad band of positive correlations across the central and east Pacific and of negative correlations in a typical "horseshoe" pattern from the subtropics through the tropical western Pacific (Fig. 8a). On the other hand, the positive correlations extend too much westward and are confined to the Tropics, while the horseshoe SST pattern in the extra-tropical Pacific is not realistic in CNRM-CM5, particularly in the North Pacific (Fig. 8b). The narrow equatorial confinement of the positive SST anomalies is consistent with the unrealistic high ENSO frequency in CNRM-CM5 (see Fig. 6a; Kirtman, 1997; Davey et al., 2002). In the Indian Ocean, CNRM-CM5 simulates a too strong Indian Ocean Dipole variability during fall season (Saji et al., 1999) in response to El Niño events, with the negative correlations extending too far west into the equatorial Indian Ocean, confining the positive teleconnection signal to the far west of that basin. Due to the incorrect phase locking of ENSO variability to the annual cycle in IPSL-CM5, the corresponding seasonal evolution of the SST correlation patterns is unrealistic with positive correlations in the tropical Indian and Pacific oceans observed from February-March to December-January seasons (Fig. 8c).

c. ISM variability

As a first basic assessment of ISM variability, the monthly standard-deviations of ISM rainfall area-averaged over India (70°-95°E, 5°-30°N) for the GPCC, GPCP datasets and all configurations of the two coupled models are shown in Figure 9. In the observations (both GPCC and GPCP), the rainfall variability is low outside the summer monsoon season and peaks during the onset and withdrawal phases of the monsoon. On the other hand, ISM rainfall standard deviations are quite higher in CNRM-CM3 during pre- and post-monsoon seasons with also a wider spread inside boreal summer (Fig. 9a). Both problems have been partly corrected in the CMIP5 version. Similar improvements from CMIP3 to CMIP5 are also observed for the IPSL model, since the rainfall standard deviations have now the correct amplitude during ISM, even though the delay of the ISM onset already observed over the ISM rainfall annual cycle is also seen here on the cycle of ISM rainfall variability (Fig. 9b). Such improvements from CMIP3 to CMIP5 are consistent with the patterns of ISM rainfall variability illustrated in Fig. 5 in which the biases over the Indian subcontinent have been reduced in the current versions of both models.

To further elucidate the ISM rainfall variability, Figure 10 shows the power spectra of ISM rainfall time series during boreal summer (JJAS average over land) in the observations and the different available simulations from the two models. Interestingly, the observed ISM rainfall time series is not basically biennial as it is assumed by many studies (Yasunari, 1990; Meehl and Arblaster, 2002), but rather exhibits a triennial oscillation as many monsoon indicators (Bhalme and Jadhav, 1984). Focusing now on the model's outputs, we first observed that the dominant time scales of ISM rainfall variability varied considerably and significantly between the different members of the CMIP5 historical simulations of the two models, while such "internal" variability of frequency is not observed in the spectra of the simulated Niño-34 SST time series in both models (compare Figs. 6 and 10). Focusing now on the comparison between CMIP3 and CMIP5 versions, the results highlight that the current versions of the models are in better agreement with observations as far as the dominant time scales of ISM rainfall interannual variability is concerned. Taking into account the strong relationship between ISM rainfall variability and ENSO (see below), this result is consistent with the improvement of the spectral signature of Niño-34 SSTs in the current versions of the two models as discussed in the previous paragraph.

d. ISM and ENSO relationships

Numerous studies have shown that El Niño/La Niña is associated with a weakening/strengthening of the Indian monsoon with an over-all reduction/increase in rainfall (Webster et al., 1998; Wang, 2006; among many others). The monsoon circulation anomalies associated with ENSO are either driven remotely by teleconnections through changes in the Walker circulation, or locally by anomalous heating or air-sea interactions. Such teleconnections between ISM and ENSO are indeed responsible for the main modes of rainfall interannual variability observed over India and the tropical Indian Ocean. It is therefore extremely important to examine if the ENSO-ISM relationships are well simulated in state-of-the art CGCMs (Annamalai et al., 2007; Terray et al., 2005a, 2011). Here, we are evaluating the relationship between ENSO and ISM in both the CMIP3 and CMIP5 versions of the CNRM and IPSL models.

In order to see if the two models represent the timing of the relationship correctly, Figure 11 shows the lead-lag relationships between the two phenomena in an extended window, e.g. the 36-month evolution of the correlation between ISM rainfall/dynamical indices and monthly Niño-3.4 SSTs for observations (black line), the CMIP3 (blue line) and CMIP5 (red line), configurations of the two coupled models, starting from the beginning of the previous year (e.g. year -1) to the end of the following year of the monsoon (e.g. year +1). The Niño-3.4 domain is chosen since in observations the strongest correlations between ISM rainfall and SSTs occur over this region of the Pacific (see Fig. 12). X-axis indicates calendar month for a 36 months period starting one year before the developing year of ISM and Y-axis is the amplitude of the correlation. The dashed lines indicate the 99% significance level according to a two-tailed student t-test.

Two distant significant correlation peaks are noted in the observations (Fig. 11). Weak positive correlations are evident a year before the monsoon. Theses positive correlations preceding the monsoon have largely amplified during recent decades (e.g. after the 1976/77 climate shift) and have been the subject of several recent publications (Yang et al., 2007; Boschat et al., 2010, 2011; among others). The correlations switch sign around February-March and become significant only in April-May as a manifestation of the ENSO spring predictability barrier (Webster and Yang, 1992; Webster et al., 1998). These significant negative correlations between Niño-3.4 SSTs and ISM rainfall and dynamical indices grow steadily during the summer monsoon and fade away progressively after the boreal summer, during the peaking and decaying phases of El Niño, to cross the zero line at the onset of the monsoon the next year. The strong and significant negative correlation between ISM rainfall and SSTs over eastern and central Pacific during summer of year 0 implies that warmer (cooler) SSTs over these regions will suppress (enhance) monsoon rainfall over India during boreal summer (e.g. Webster et al., 1998). The observed maximum correlation after the monsoon season has also led to suggestions that variations in the intensity of the monsoon can potentially influence the surface wind-stress over the equatorial Pacific and thereby modify the statistical properties of ENSO (e.g., Kirtman and Shukla 2000; Wu and Kirtman, 2003).

Nearly all the versions of the models are able to reproduce the synchronous negative correlation (during boreal summer) between ISM and ENSO, though with varying amplitude. However, before and after the monsoon season, nearly all the versions of the coupled models show large discrepancies from observations, excepted perhaps the CMIP5 version of the CNRM model. Consistent with the less energetic ENSO in CNRM-CM5 (Figs. 6 and 7), the amplitude of the synchronous correlation between monthly Niño-3.4 SST and ISM rainfall is reduced compared to the CNRM-CM3 (Figs. 11a). However, the timing of the relationship between the two phenomena is also completely dissimilar from CNRM-CM3 to CNRM-CM5, with large improvements in CMIP5 configuration. In CNRM-CM3, ISM is linked to ENSO before ISM onset rather during and after ISM, the maximum negative correlation occurring the year before ISM and just before ISM onset for both the ISM rainfall and dynamical indices (Figs.11ab). Moreover, after ISM onset, the amplitude of the negative correlation quickly fades away in complete disagreement with the observed correlations. On the other hand, despite of a reduced amplitude for the ISM rainfall and Niño-3.4 SST correlations, the shape of the lead-lag correlations simulated by CNRM-CM5 perfectly matches the observational estimates with the maximum negative correlations for zero or slightly positive lags (i.e. for the ISM rainfall and dynamical indices leading the Niño-3.4 SST time series).

Furthermore, CNRM-CM5 is also able to recover the seasonal modulation of the monsoon-ENSO relationship with the slow change of sign of the correlations from positive to negative from year -1 to year 0 as observed. Focusing now on the IPSL model, both the CMIP3 and CMIP5 versions show the same deficiencies with significant negative correlations with the Niño-3.4 SSTs before rather than synchronous and after the ISM (Figs. 11bd). Obviously, the incorrect annual phase locking of the ENSO's variability (Fig. 7b) is a plausible candidate for explaining the current failure of IPSL-CM5 with respect to the simulation of the ISM-ENSO lead-lag relationships. However, even IPSL-CM3, that has a quite better representation of the tropical Pacific and the associated ENSO variability, failed to reproduce the lead-lag relationships between ISM and ENSO (Figs. 11bd). This suggests that many factors may be necessary to faithfully reproduce the ISM-ENSO relationship in CGCMs.

In order to provide a broader perspective of the performance of the two CGCMs with respect to the ISM-SST relationships, Figure 12 shows the lead-lag correlations between 2-month averaged Indo-Pacific SSTs and ISM rainfall for observations and the two models. For the sake of brevity we show again these diagnostics only for the CMIP5 model's configurations. The correlations are calculated beginning in February-March prior to the monsoon season and ending in December-January after the monsoon. As can be seen, the two coupled models exhibit a robust teleconnection pattern over the equatorial Pacific similar to observations during boreal summer.

The correspondence between the IPSL model and the observations is surprisingly overall very good during the development stage of El Niño events despite significant differences in the simulated and observed early evolution of ENSO in the equatorial Pacific (errors which are consistent with the lead-lag correlations between Niño-3.4 SSTs and ISM rainfall displayed in Fig. 11). The observed correlation patterns before the El Niño onset suggests the importance of extratropical latitudes, with possible precursory SST signals stemming from the North Pacific and South Indian regions during February-March (Fig. 12a; Terray et al., 2005b; Peings et al., 2009). Interestingly, the IPSL model is able to recover the SST precursory pattern found in the North Pacific region, which takes the form of a warm C-shaped 'footprint' during AM both in observations and IPSL-CM5 (Fig. 12c; Vimont et al., 2003). Consistent with the Tropospheric Biennial Oscillation pattern documented by Meehl and Arblaster (2002), negative correlations are simulated in the western Indian Ocean and positive correlations in the eastern Indian Ocean by both IPSL-CM5 and observations during the late boreal summer and fall. However, these regional signals are much stronger in observations. Moreover, a weak (strong) monsoon is followed by the peak phase of the El Niño (La Niña) event with the development of the traditional "horseshoe" pattern characteristic of ENSO in the Pacific and a large warm (cold) SST anomaly over the Indian Ocean associated with the weaker monsoon flow both in observations and IPSL simulations (Figs. 12ac). Thus, IPSL-CM5 captures the main SST-ISM teleconnections even though the negative correlations in the equatorial Pacific are too meridionally confined and the positive correlations in the subtropical Pacific are much too weak and not well-simulated during ISM and the following boreal fall and winter. This is rather surprising taking into account the incorrect phase-locking of ENSO variability to the annual cycle in IPSL-CM5 (Fig. 7b).

Despite of the fact the CNRM-CM5 captures the observed phase-locking of Niño-3.4 SST anomalies with the seasonal cycle (Fig. 7a) and the seasonal evolution of the correlations between monthly Niño-3.4 SST and ISM rainfall (Figs. 11ac), CNRM-CM5 does not represent the magnitude of the association between Indo-Pacific SSTs and ISM rainfall anomalies correctly (Fig. 12b). The shortcomings of CNRM-CM5 are particularly evident during boreal spring and summer since the significant correlations are only restricted to the central equatorial Pacific in the CNRM simulations during these seasons. From boreal fall to winter after the monsoon, the positive correlations forming the two branches of the traditional ENSO horseshoe pattern in the Pacific are also much less intense and not properly simulated in CNRM-CM5. These problems related to the CNRM model are evident in the mean correlation patterns displayed in Fig. 12b as well as in the correlation maps computed from each of the ten simulation members separately (not shown, there is some inter-member variability in the correlations and therefore a smoothing effect of the ensemble averaging but all members underestimate the magnitude of the observed correlations). Furthermore, the same deficiency is found if we use the ISM dynamical index instead of the ISM rainfall time series in the correlation analysis (not shown).

To further elucidate the relationships between ENSO and ISM rainfall, we finally assess the changes in correlation between ISM rainfall and JJAS Niño-3.4 SST time series by computing them in 21-yr sliding window for the CMIP5 experiments of the two models whose length is exactly comparable to the observed record and which include both the anthropogenic and natural forcings as in the observed climate (Fig. 13).

There are clear decadal changes in ENSO-monsoon teleconnections in observations during the 20th century (e.g., Webster et al. 1998, Torrence and Webster, 1999; Krishnamurthy and Goswami, 2000). ENSO-monsoon teleconnections are weak at the early (before 1930) and end of 20th century and strong between the two periods, during 1935 to 1970. Moreover, the drop in synchronous correlations between ENSO and ISM rainfall observed during recent decades is still a matter of intense debate and there have been attempts to understand the plausible reasons for this recent low-frequency modulation of the monsoon-ENSO relationship (Krishna Kumar et al., 1999; Krishnamurthy and Goswami, 2000; Chang et al., 2001; Gershunov et al., 2001; Kinter et al., 2002; Annamalai et al., 2007; Kucharski et al., 2007). Especially, Krishna Kumar et al. (1999) suggested that the mid-latitude continental warming (in relation to the global warming) favors the enhanced land–ocean thermal gradient conducive to a strong monsoon and, thus, helps to sustain the ISM rainfall at a normal level despite strong ENSO events during recent decades.

Epochs with a highly significant out-of-phase ISM-ENSO correlation (-0.8) alternate with periods in which these correlations are very modest (-0.2) in both the observations and *individual members* of the model's outputs (Fig. 13). Interestingly, there is also a larger spread in CNRM-CM5 within the different members as compared to IPSL-CM5. However, these epochal/decadal changes in teleconnections are not reproduced in the ensemble mean response of the two models, which suggests a stationary relationship between ISM and ENSO in the global warming context of the 20th century. Especially during the recent decades when the anthropogenic forcing is the strongest and the observed ISM-ENSO relationship is the weakest in the observed record, there are no significant changes of the ISM-ENSO relationships in the ensemble mean of the two models. Furthermore the same results are obtained if an ISM dynamical index is used in the sliding correlation analysis (not shown). These results are consistent with the conclusions of Gershunov et al. (2001) and Annamalai et al. (2007) and suggest that the recent weakening of the ISM-ENSO correlation is probably related the intrinsic stochastic nature of the link between ISM and ENSO and not to the global warming forcing as first suggested by Krishna Kumar et al. (1999).

5. Conclusions and discussion

The present study is aimed at evaluating the CMIP5 simulations made by the two French state-of-the-art CGCMs with ten and four historical coupled simulations for, respectively, the CNRM and IPSL CGCMs, both driven by natural and anthropogenic forcings. The focus is to document the evolution of these coupled models from CMIP3 to CMIP5 and to compare the performance of these models in their ability to simulate ISM rainfall, its variability and its relationship with ENSO. Despite of the fact that the two CGCMs share the same ocean component, they display a wide range of skill in simulating the tropical mean state, ISM, ENSO and their reciprocal relationships.

Even after improving the physics (for CNRM) or increasing the spatial and vertical resolutions (for CNRM and IPSL) in the CGCMs, the results are not up to mark with progresses in simulating some aspects of the tropical climate variability, but also degradations on some others. The large systematic errors affecting the rainfall and SST boreal summer climatologies in CNRM-CM3 have been largely reduced in CNRM-CM5. In particular, the large cold SST bias found in the Tropics and Subtropics in CNRM-CM3 has been largely corrected in CNRM-CM5 by changes in the atmosphere and ocean parameterized physics. Surprisingly and despite of the fact that the physics of the CMIP3 and CMIP5 versions of the IPSL model (in the atmosphere) are identical, this model in its current version exhibits a more pronounced double ITCZ in rainfall and a colder tongue in equatorial SSTs over the tropical Pacific with an erroneous annual cycle in the eastern tropical Pacific. However, both models now capture the broad features of the monsoon over the India with respect to the annual cycle of rainfall and dynamical indices. Especially, the monsoon rainfall climatology is far better in IPSL-CM5 than in IPSL-CM3 simulations despite of the fact that ISM onset and peak are delayed by one month in the current version.

The periodicity of the simulated ENSO is now fairly realistic in the IPSL model, thanks to the increased spatial and vertical atmospheric resolutions (Guilyardi et al., 2004), but IPSL-CM5 fails to simulate the phase-locking of ENSO with respect to the annual cycle, with El Niño events peaking in boreal spring instead of boreal winter. This error is probably related to the erroneous annual cycle generated in the eastern tropical Pacific, which is also an unexpected outcome from the increased spatial and vertical resolutions of the atmospheric component in IPSL-CM5. Changes in atmosphere and ocean parameterized physics have also improved the simulated spectral characteristics and the amplitude of ENSO variability in CNRM-CM5. The simulated ENSO in the CNRM model has now the correct amplitude, but is still too regular, with a too short time scale compared to the observations. Moreover, this model faithfully reproduces the phase locking of ENSO with respect to the annual cycle, which is of paramount importance for a realistic simulation of the lead-lag relationships between ISM rainfall and ENSO. Both IPSL-CM5 and CNRM-CM5 fail however to capture all the details of ENSO-related SST variability such as the meridian extent of the SST anomalies in the eastern Pacific or the observed SST horseshoe pattern in the extra-tropical Pacific and tend to produce SST anomalies that extend too far into the western tropical Pacific as many other CGCMs (AchutaRao and Sperber, 2006).

Nearly all versions of the models are able to reproduce the synchronous negative correlation (during boreal summer) between ISM and ENSO, though with varying amplitude. However, before and after the monsoon season, nearly all the versions of the coupled models show large discrepancies from observations, excepted perhaps CNRM-CM5. In particular, CNRM-CM3 and the two versions of the IPSL model show significant and large negative correlations before the monsoon which are completely absent in the observational estimates. In a similar fashion, the simulated correlations fade away quickly after the ISM onset and are much weaker than observed suggesting that the two CGCMs are not able to reproduce the impact of anomalous monsoons on La Niña or El Niño events in the Pacific (Kirtman and Shukla 2000; Wu and Kirtman, 2003).

Thus, the CMIP3 CGCMs, including the two CGCMs considered here, show large discrepancies from the observations with respect to the simulation of the complex leag-lag relationships between ISM and ENSO which is central to seasonal prediction for South Asia (Annamalai et al., 2007; Terray et al., 2011). Taking into account the overall improvement of the mean state, seasonal cycle and interannual variability in the tropical Pacific simulated by the CMIP3 models (AchutaRao and Sperber, 2006), the reasons for this general failure of current CGCMs in simulating the monson-ENSO teleconnections are not clear. One plausible reason is that, despite a large diversity of simulated ENSO, most coupled models still have difficulty to reproduce the phase-locking of east Pacific SST variability to the annual cycle which is central in capturing the monsoon-ENSO relationship (Turner et al., 2005). However, it is worth noting that even CGCMs performing well in their representation of the annual cycle of Niño-34 SST variability do not perform significantly better in recovering the monsoon-ENSO relationship. This is well illustrated in the present study by the case of the CMIP3 and CMIP5 versions of the IPSL model which exhibit similar lead-lag correlations between ISM rainfall and ENSO despite significant differences in the phase-locking of ENSO to the annual cycle.

In IPSL-CM5, the amplitude of the ENSO teleconnection is comparable to the observations, but the timing of this teleconnection is still incorrect, peaking before the ISM onset rather than during and after ISM as observed, despite of significant improvements in monsoon climatology. As a result of significant improvements in the simulation of ENSO characteristics, CNRM-CM5 is now able to capture many aspects of the observed lead-lag relationships between ISM rainfall and El Niño events. However, the strength of the ENSO teleconnection during the boreal summer is significantly reduced in CNRM-CM5 compared to observations and is restricted to the central equatorial Pacific. This suggests that this model is not able to simulate realistic SST-ISM teleconnections in the Indo-Pacific areas. Overall, the results from CMIP5 simulations suggest that progresses or changes in the simulation of the ISM-ENSO relationships in the two CGCMs can be traced back to modifications of ENSO characteristics in the new simulations and that the monsoon rainfall climatology only plays a secondary role.

Generally speaking, it is however very difficult to attribute differences between the CMIP3 and CMIP5 model versions without a systematic assessment of each individual modification. In this respect, the present study is somewhat frustrating, but is probably another good illustration of the increasing gap between simulation and understanding in climate modeling (Held, 2005). Model development should probably be even more central in CMIP and each model component (atmosphere and ocean, but also land, sea-ice, etc…) should be also evaluated in off-line mode in order to better understand the reasons behind the improvements (or degradations) between successive CMIP exercises. One suggestion would be that intercomparison projects for individual components should be linked (or even embedded) to (in) CMIP. In this respect, CMIP5 has made a step forward since AMIP-type atmospheric simulations driven by observed SST have been required from each modeling center. Such simulations have not been analyzed in the present study since ENSO is fundamentally a coupled ocean-atmosphere phenomenon. Nevertheless, preliminary analyses conducted at CNRM indicate that some features of the Indian monsoon are better simulated in CMIP versus AMIP runs. Such a result raises another crucial issue, indeed the possibility of error cancellation in coupled models and/or the fact that most modeling centers still develop and tune their atmospheric component in AMIP mode (e.g. Hazeleger et al. 2010) while climate variability, especially in the tropics, is dominated by coupled ocean-atmosphere processes.

Finally, coming back to the ENSO-monsoon relationship and in line with former modeling studies, both CNRM and IPSL CMIP5 models show a strong multi-decadal modulation of the 20th century ISM rainfall-ENSO correlations in individual members of the historical simulations of both models, but no systematic (i.e. ensemble mean) change with increasing amounts of greenhouse gases, thereby suggesting a stationary ISM-ENSO relationship during the last century. The CMIP5 projections of CNRM and IPSL are beyond the scope of the present study, but preliminary analyses confirm the stationnarity of the simulated relationship over the 21st century.

Acknowledgments: Financial support from the Indo-French CEFIPRA project (N° 3907/1) is acknowledged. The GPCP and HadISST1.1 datasets were provided by the NOAA–CIRES Climate Diagnostics Center from the Web site (http://www.cdc.noaa.gov). We gratefully acknowledge the outstanding work undertaken at Météo-France, IPSL and CERFACS in the framework of CMIP5. This acknowledgement is extended to the many international modeling groups who provided their numerous model experiments for the Program for Climate Model Diagnosis and Intercomparison (PCMDI). For more details on model data or documentation for CMIP3 and CMIP5, readers are referred to the PCMDI Web site (http://www-pcmdi.llnl.gov).

References

Achutarao K, Sperber, KR (2002) Simulation of the El Niño Southern Oscillation: Results from the Coupled Model Intercomparison Project. Clim Dyn 19:191-209.

AchutaRao K, Sperber, KR (2006) ENSO simulation in coupled ocean-atmosphere models: are the current models better? Clim Dyn 27:1-15.

Alexander MA, Bladé I, Newman M, Lanzante JR, Lau NC, Scott JD (2002) The atmospheric bridge: The influence of ENSO teleconnections on air–sea interaction over the global oceans. J Clim 15:2205–2231.

Amman, C.M., F. Joos, D.S. Schimel, B.L. Otto-Bliesner, R.A. Tomas, (2007) Solar influence on climate during the past millennium: results from transient simulations with the NCAR climate system model. Proc Natl Acad. Sci., 104: 3713-3718.

Annamalai H, Hamilton K, Sperber KR (2007) South Asian summer monsoon and its relationship with ENSO in the IPCC AR4 simulations. J Clim 20:1071–1092.

Ann S.-I., Wang KR (2000) Interdecadal change of the structure of ENSO mode and its impact on the ENSO frequency. J Clim, 13:2044-2055.

Ashrit RG, Douville H, Rupa Kumar K (2003) Response of Indian monsoon and ENSO-monsoon teleconnection to enhanced greenhouse effect in the CNRM coupled model. J Meteoro Soc Japan 81:779–803.

Bhalme HN, Jadhav SK (1984) The Southern Oscillation and its relation to the monsoon rainfall. Int. J. of Climatology 4:509-520.

Boschat G, Terray P, Masson S (2010) Interannual relationships between Indian Summer Monsoon and Indo-Pacific coupled modes of variability during recent decades. Clim Dyn doi:10.1007/s00382-010-0887-y.

Boschat G, Terray P, Masson S (2011) Robustness of SST teleconnections and precursory patterns associated with the Indian Summer Monsoon. Clim Dyn 10.1007/s00382-011-1100-7.

Chang CP, Patrick Harr, Jianhua Ju (2001) Possible Roles of Atlantic Circulations on the Weakening Indian Monsoon Rainfall–ENSO Relationship. J Clim 14:2376–2380.

Cleveland RB, Cleveland WS, McRae JE, Terpenning I (1990) A Seasonal-Trend Decomposition Procedure Based on Loess (with Discussion). Journal of Official Statistics 6:3-73.

Covey C, AchutaRao KM, Cubasch U, Jones P, Lambert SJ, Mann ME, Phillips TJ, Taylor KE (2003) An overview of results from the Coupled Model Intercomparison Project. Global Planet. Change 37:103–133.

Cubasch U, G.A. Meehl GA, Boer GJ, Stouffer RJ, Dix M, Noda A, Senior CA, Raper S Yap KS (2001) Projections of future climate change. Climate Change 2001: The Scientific Basis. Contribution of Working Group I to the Third Assessment Report of the Intergovernmental Panel on Climate Change, Houghton JT, Ding Y, Griggs DJ, Noguer M, van der Linden PJ, Dai X, Maskell K Johnson CA, Eds., Cambridge University Press, Cambridge, 525-582.

Dai A (2006) Precipitation Characteristics in Eighteen Coupled Climate Models. J Clim 19:4605–4630. doi: 10.1175/JCLI3884.1.

Davey MK., M. Huddleston M, Sperber KR, Power SB, Colman RA, Flato G, Kimoto M, L. Terray L, DeWitt D, Roeckner E, Oberhuber J, Voss R, Cubasch U, Knutson TR, Manabe S, Wang B, Fairhead L, Le Treut H, Vintzileos A, Delecluse P, Braconnot P, I. Yoshikawa I, Chen D, Zebiak SE, Gordon C, Cooper C, Latif M, Yukimoto S, Kitoh A, F. Bryan F, G.A. Meehl GA, Washington WM, Ji M, Hogan T, Li T, Yu JY, C. R. Mechoso (2000) STOIC: A study of coupled GCM climatology and variability in tropical ocean regions. Clim Dyn 18:403–420.

Delecluse P, Davey MK, Kitamura Y, Philander SGH, Suarez M, Bengtsson L (1998) Coupled general circulation modelling of the Tropical Pacific, J Geophys Res, 103(C7): 14357-14373.

Dufresne et al., (2012) Overview of the IPLS-CM5 Earth System Model with an emphasis on model and forcing changes between CMIP3 and CMIP5, Climate dynamics, this issue.

Ebisuzaki W (1997) A method to estimate the statistical significance of a correlation when the data are serially correlated. J Clim 10:2147-2153.

Gadgil S, Sajani S (1998) Monsoon precipitation in the AMIP runs. Clim Dyn 14:659-689.

Gates WL (1992) AMIP: the Atmospheric Model Intercomparison Project. Bull Amer Meteor Soc 73:1962-1970.

Gershunov A, Schneider N, Barnett T (2001) Low-frequency modulation of the ENSO-Indian monsoon rainfall relationship: signal or noise? J Clim 14:2486-2492.

Guilyardi E, Gualdi S, Slingo JM, Navarra A, Delecluse P, Cole J, Madec G, Roberts M, Latif M, Terray L (2004): Representing El Niño in coupled ocean-atmosphere GCMs: the dominant role of the atmospheric component. J Clim, 17:4623-4629.

Guilyardi E, Wittenber A, Fedorov A, Collins M, Wang C (2009) Understanding El Niño ocean-atmosphere General Circulation Models. Bull Amer Meteor Soc 90:325-340.

Hazeleger W. et al. (2010) EC-Earth: A Seamless Earth-System Prediction Approach in Action. Bull. Amer. Meteor. Soc., 91:1357-1363.

Held, I.M. (2005) The Gap between Simulation and Understanding in Climate Modeling. Bull. Amer. Meteor. Soc., 86, 1609–1614.

Huffman, George J, Robert F Adler, Mark M Morrissey, David T Bolvin, Scott Curtis, Robert Joyce, Brad McGavock, Joel Susskind (2001) Global Precipitation at One-Degree Daily Resolution from Multisatellite Observations. J Hydrometeor 2:36–50.

Kinter JL, Miyakoda K, Yang S (2002) Recent change in the connection from the Asian monsoon to ENSO. J Clim 15:1203–1215.

Kirtman BP (1997) Oceanic Rossby waves dynamics and the ENSO period in a coupled model. J Clim 10:1690-1704.

Kirtman BP, Shukla J (2000) On the influence of the Indian summer Monsoon on ENSO. Quart J Roy Meteor Soc 126:213-239.

Kripalani RH, Oh JH, Kulkarni A, Sabade SS, Chaudhari HS (2007) South Asian summer monsoon precipitation variability: coupled climate model simulations and projections under IPCC AR4. Theor Appl Climatol 90:133–159.

Krishnamurthy V, Goswami BN (2000) Indian monsoon–ENSO relationship on interdecadal timescale. J Clim 13:579–594.

Kucharski F, Bracco A, Yoo JH Molteni F (2007) Low frequency variability of the Indian Monsoon – ENSO relation and the Tropical Atlantic. The 'weakening' of the '80s and '90s. J Clim 20:4255-4266.

Kucharski F, Scaife AA, Yoo JH, Folland CK, Kinter J, Knight J, Fereday D, Fischer AM, Jin E, Kroger J, Lau NC, Nakaegawa T, Nath MJ, Pegion P, Rozanov E, Schubert S, Sporyshev PV, Syktus S, Voldoire A, Yoon JH, Zeng N, Zhou T (2009) The CLIVAR C20C Project. Skill of simulating Indian monsoon rainfall on interannual to decadal timescales. Does GHG forcing play a role?" Clim Dyn 33:615-627.

Kumar KK, Rajagopalan B, Cane MA (1999) On the weakening relationship between the Indian Monsoon and ENSO. Science 284:2156–2159.

Kumar, KK, Kamala K, Rajagopalan B, Hoerling MP, Eischeid JK, Patwardhan SK, Srinivasan G, Goswami BN, Nemani R (2010) The once and future pulse of Indian monsoonal climate. Climate Dynamics 36:2159-2170.

Lin, Jia-Lin (2007a) The Double-ITCZ Problem in IPCC AR4 Coupled GCMs: Ocean–Atmosphere Feedback Analysis. J Clim 20:4497–4525.

Lin, Jia-Lin (2007b) Interdecadal variability of ENSO in 21 IPCC AR4 coupled GCMs. Geo Res Lett, 34:L12702, doi:10.1029/2006GL028937.

Madec G (2008) NEMO ocean engine. Note du Pole de modélisation, Institut Pierre-Simon Laplace (IPSL), France, No 27 ISSN No 1288-1619.

Manabe S, Bryan K (1969) Climate calculations with a combined ocean-atmosphere model. J Atm Sci 26 :786–789.

Manganello JV, Huang B (2009) The influence of systematic errors in the Southeast Pacific on ENSO variability and prediction in a coupled GCM. Clim Dyn 32:1015-1034.

Marti O, Braconnot P, Bellier J, Benshila R, Bony S, Brockmann P, Cadule P, Caubel A, Denvil S, Dufresne JL, Fairhead L, Filiberti MA, Foujols MA, Fichefet T, Friedlingstein P, Gosse H, Grandpeix JY, Hourdin F, Krinner G, Lévy C, Madec G, Musat I, de Noblet N, Polcher J, Talandier C (2006) The new IPSL climate system model. IPSL-CM4. Note du Pôle de Modélisation, n. 26: ISSN 1288-1619, available at the website:

http://dods.ipsl.jussieu.fr/omamce/IPSLCM4/DocIPSLCM4/HTML/

Mechoso CR, Robertson AW, Barth N, Davey MK, Delecluse P, Gent PR, S. Ineson S, B. Kirtman B, Latif M, Le Treut H, Nagal T, Neelin JD, Philander SGH, Polcher J, Schopf PS, Stockdale T, Suarez MJ, Terray L, Thual O, Tribbia JJ (1995) The seasonal cycle in the Tropical Pacific in Coupled Ocean-Atmsphere General Circulation Models. Mon Weath Rev 123:2825-2838.

Meehl, GA (1995) Global coupled general circulation models. Bull Amer Meteor Soc 76: 951–957.

Meehl GA, Boer GJ, Covey C, Latif M, Stouffer RJ (1997) Intercomparison makes for a better climate model. Eos Trans Amer Geophys Union 78:445–446.

Meehl GA, Boer GJ, Covey C, Latif M, Stouffer RJ (2000) The Coupled Model Intercomparison Project (CMIP). Bull Amer Meteor Soc 81:313–318.

Meehl GA, Gent, PR, Arblaster JM, Otto-Bliesner BL, Brady EC, Craig A (2001) Factors that affect the amplitude of El Niño in global coupled climate models. Clim Dyn 17: 515-526.

Meehl GA, Arblaster J (2002) The tropospheric biennial oscillation and the Asian-Australian monsoon rainfall. J Clim 15:722-744.

Meehl GA, Stocker TF, Collins WD, Friedlingstein P, Gaye AT, Gregory JM, Kitoh A, Knutti R, Murphy JM, Noda A, Raper SCB, Watterson IG, Weaver AJ, Zhao ZC (2007a) Global Climate Projections. In: Climate Change 2007: The Physical Science Basis. Contribution of Working Group I to the Fourth Assessment Report of the Intergovernmental Panel on Climate Change [Solomon, S., D. Qin, M. Manning, Z. Chen, M. Marquis, K.B. Averyt, M.Tignor and H.L. Miller (eds.)]. Cambridge University Press, Cambridge, United Kingdom and New York, NY, USA.

Meehl Gerald A, Covey Curt, Delworth, Thomas, Latif, Mojib, McAvaney, Bryant, Mitchell, John FB, Stouffer, Ronald J, Taylor, Karl E (2007b), The WCRP CMIP3 multimodel dataset: A new era in climate change research, Bull Amer Meteorol Soc 88:1383–1394.

Meehl GA, Bony S (2011) Introduction to CMIP5. CLIVAR Exchanges No. 56:16(2).

Peings Y, Douville H, Terray P (2009) Extended winter Pacific North America oscillation as a precursor of the Indian summer monsoon rainfall. Geophys Res Lett 36:L11710. Doi: 10.1029/2009GL038453.

Rasmusson EM, Carpenter TH (1983) The relationship between eastern equatorial Pacific sea surface temperature and surface wind fields associated with the Southern Oscillation/El Niño. Mon Weather Rev 111:517–528.

Rayner NA, Parker DE, Horton EB, Folland CK, Alexander LV, Rowell DP, Kent EC, Kaplan A (2003) Global analyses of sea surface temperature, sea ice, and night marine air temperature since the late nineteenth century. J Geophys Res 108:4407, doi:10.1029/2002JD002670.

Rudolf B, Beck C, Grieser J et Schneider U (2005) Global Precipitation Analysis Products. Global Precipitation Climatology Centre (GPCC), DWD, Internet publication, 1-8.

Saji NH, Goswami BN, Vinaychandran PN, Yamagata Y (1999) A dipole mode in the Tropical Indian Ocean. Nature 401:360–363.

Salas-Mélia D., F. Chauvin, M. Déqué, H. Douville, J-F. Guérémy, P. Marquet, S. Planton, J.F. Royer and S. Tyteca (2005) Description and validation of the CNRM-CM3 global coupled model. Note de Centre du CNRM, n°103.

Shukla, J, Hagedorn R, Hoskins B, Kinter J, Marotzke J, Miller M, Palmer TN, Slingo J (2009) Strategies: Revolution in Climate Prediction is Both Necessary and Possible: A Declaration at the World Modelling Summit for Climate Prediction. Bull Amer Meteor Soc 90:175–178.

Sun Y, Ding Y, Dai A (2010) Changing links between South Asian summer monsoon circulation and tropospheric land-sea thermal contrasts under a warming scenario. Geo Res Lett 37:L02704, doi:10.1029/2009GL041662.

Szopa S. A. Cozic, M. Shulz, Y. Balkanski, D. Hauglustaine (2012) Changes in tropospheric aerosol and reactive gases burdens and concentrations under IPCC-AR5 emission scenarios for 1850-2100. Climate Dynamics, this issue.

Terray P, Guilyardi E, Fischer AS, Delecluse P (2005a) Dynamics of the Indian Monsoon and ENSO Relationships in the SINTEX global Coupled Model. Clim Dyn 24:145-168.

Terray P, Dominiak S, Delecluse P (2005b) Role of the southern Indian Ocean in the transitions of the monsoon-ENSO system during recent decades. Clim Dyn 24:169–195.

Terray et al, (2011) The role of the intra-daily SST variability in the Indian Monsoon variability and monsoon-ENSO-IOD relationships in a global coupled model. Submitted to Climate Dynamics.

Torrence C, Webster PJ (1999) Interdecadal changes in the ENSO-Monsoon System. J Clim 12:2679-2690.

Turner AG, Inness PM, Slingo JM (2005) The role of the basic state in the ENSO-monsoon relationship and implications for predictability. Quart J Roy Meteor Soc 131:781–804.

Ueda H, Iwai A, Kuwako K, Hori M (2006) Impact of anthropogenic forcing on the Asian summer monsoon as simulated by eight GCMs. Geophys Res Lett 33:L06703, doi:10.1029/2005GL025336.

Uppala SM, Kållberg PW, Simmons AJ, Andrae U, da Costa Bechtold V, Fiorino M, Gibson JK, Haseler J, Hernandez A, Kelly GA, Li X, Onogi K, Saarinen S, Sokka N, Allan RP, Andersson E, Arpe K, Balmaseda MA, Beljaars ACM, van de Berg L, Bidlot J, Bormann N, Caires S, Chevallier F, Dethof A, Dragosavac M, Fisher M, Fuentes M, Hagemann S, Hólm E, Hoskins BJ, Isaksen, L, Janssen PAEM, Jenne R, McNally AP, Mahfouf JF, Morcrette JJ, Rayner NA, Saunders RW, Simon P, Sterl A, Trenberth KE, Untch A, Vasiljevic D, Viterbo P, Woollen J (2005) The ERA-40 re-analysis. Quart. J R Meteorol Soc 131:2961-3012.doi:10.1256/qj.04.176

Vimont DJ, Wallace JM, Battisti DS (2003) The seasonal footprinting mechanism in the Pacific: implications for ENSO. J Clim 16:2668-2675.

Voldoire A, E. Sanchez-Gomez, D. Salas y Mélia, B. Decharme, C. Cassou, S.Sénési, S. Valcke, I. Beau, A. Alias, M. Chevallier, M. Déqué, J. Deshayes, H. Douville, E. Fernandez, G. Madec, E. Maisonnave , M.-P. Moine, S. Planton, D.Saint-Martin, S. Szopa, S. Tyteca, R. Alkama, S. Belamari, A. Braun, L. Coquart, F. Chauvin (2012) The CNRM-CM5.1 global climate model: description and basic evaluation. Climate Dynamics, this issue.

von Storch H, Zwiers FW (1999) Statistical Analysis in Climate Research. Cambridge University Press, 484 pp, ISBN 0521 450713.

Wang B (1995) Interdecadal changes in El Niño onset in the last four decades. J Clim 8:267–285.

Wang B (2006) The Asian Monsoon. Springer- Verlag/Praxis Publishing, New York, 787 pp.

Wang B, Renguang W, Lau KM (2001) Interannual Variability of the Asian Summer Monsoon: Contrasts between the Indian and the Western North Pacific-East Asian Monsoons. J Clim 14(20):4073-4090.

Webster PJ, Magana VO, Palmer TN, Shukla J, Tomas RA, Yanai M, Yasunari T (1998) Monsoons: Processes, predictability and the prospects for prediction. J Geophys Res, 103(C7):14451–14510.

Webster PJ, Yang S (1992) Monsoon and ENSO: Selectively interactive systems. Quart. J. Roy. Meteor. Soc., 118:877-926.

Welch PD (1967) The use of Fast Fourier Transform for the estimation of power spectra: a method based on time averaging over short, modified periodograms. IEEE Transactions on Audio and Electroacoustics, 15:70-73.

Wittenberg AT (2009). Are historical records sufficient to constrain ENSO simulations. Geophys. Res. Lett 36:1-5,L12702.

Wu R, Kirtman BP (2003) On the impacts of the Indian summer monsoon on ENSO in a coupled GCM. Quart J Roy Meteor Soc 129B:3439-3468.

Yang J, Liu Q, Xie SP, Liu Z, Wu L (2007) Impact of the Indian Ocean SST basin mode on the Asian summer monsoon. Geophys Res Lett 34:L02708. Doi: 10.1029/2006GL028571.

Yasunari T (1990) Impact of Indian monsoon on the coupled atmosphere/ocean system in the tropical Pacific. Meteor & Atmos Phys 44:29-41.

Figure captions

Figure 1: ISM rainfall trend during the 20th century observed and simulated by the historical (20c3m) coupled simulations in the framework of CMIP3. The trends have been estimated with the help of the STL (Seasonal-Trend decomposition procedure based on Loess) additive scheme developed by Cleveland et al. (1990).

Figure 2: Differences between rainfall boreal summer climatology estimated from the GPCP dataset and (a) CNRM-CM3, (b) CNRM-CM5, (c) IPSL-CM3 and (d) IPSL-CM5. (e), (f), (g) and (h), same as (a), (b), (c) and (d), but for SST boreal summer climatology as observed from the HadISST dataset and simulated by the CGCMs (ensemble-mean climatologies are used for CNRM-CM5 and IPSL-CM5 when computing the differences).

Figure 3: Observed and simulated mean annual cycle of monthly rainfall averaged over land for an Indian domain (5°N–30°N/70°E–95°E) for (a) CNRM-CM3 and CNRM-CM5, (b) IPSL-CM3 and IPSL-CM5, and of the monsoon dynamical index proposed by Wang et al. (2001) for (c) CNRM-CM3 and CNRM-CM5, (d) IPSL-CM3 and IPSL-CM5. On each panel, the thick red line and red shading show, respectively, the ensemble-mean and the spread among the individual members of the historical simulations for the CMIP5 version of the models.

Figure 4: SST seasonal cycle in the Niño-34 (5°S-5°N, 170°-120°W) region derived from the HadISST dataset and the models both from the 20c3m (CMIP3) and historical (CMIP5) simulations. (a) CNRM-CM3 and CNRM-CM5, (b) IPSL-CM3 and IPSL-CM5. On each panel, the thick red line and red shading show, respectively, the ensemble-mean and the spread among the individual members of the historical simulations for the CMIP5 version of the models.

Figure 5: Differences between boreal summer rainfall standard deviations estimated from the GPCP dataset and (a) CNRM-CM3, (b) CNRM-CM5, (c) IPSL-CM3 and (d) IPSL-CM5. (e), (f), (g) and (h), same as (a), (b), (c) and (d), but for boreal summer SST standard deviations as observed from the HadISST dataset and simulated by the CGCMs (ensemble-mean standard deviations are used for CNRM-CM5 and IPSL-CM5 when computing the differences).

Figure 6: Power spectra of detrended monthly Niño-34 SST time series estimated from the observations (HadISST) and the different simulations. (a) HadISST (black line), CNRM-CM3 (blue line), CNRM-CM5 individual simulations (red line) and CNRM-CM5 ensemble-mean spectrum (green line). (b) Same as (a), but for IPSL-CM3 and IPSL-CM5. The bottom axis of

each panel is the period (unit: month), the left axis is variance (unit: °C^2) and both axes are in logarithm scale. The power spectrum is estimated using a FFT algorithm on overlapping segments (Welch, 1967) and the point-wise 99% confidence interval for the spectrum estimated from the observations is plotted in black dashed lines in each panel.

Figure 7: Monthly standard deviations of the Niño-34 SST time series from HadISST dataset and the different configurations of the two models. (a) HadISST (black line), CNRM-CM3 (blue line) and CNRM-CM5 (red line). (b) Same as (a), but for IPSL-CM3 (blue line) and IPSL-CM5 (red line). On each panel, the thick red line and red shading show, respectively, the ensemble-mean standard-deviation and the spread among the individual members of the historical simulations for the CMIP5 version of the models.

Figure 8: (a) Lagged correlations between bi-monthly averaged Indo-Pacific SSTs and the December-January Niño-3.4 SST for the HadISST dataset. The correlations are calculated beginning in February-March, prior to the El Niño onset, and ending in December-January at the peak season of El Niño events. Correlations that are above the 90% significance confidence level according to a phase-scramble bootstrap test (Ebisuzaki, 1997) are underlined. (b) Same as (a), but for CNRM-CM5. (c) Same as (a), but for IPSL-CM5. In (b) and (c), the ensemble-mean correlation patterns and critical probabilities are plotted.

Figure 9: Monthly standard deviations of ISM rainfall time series from GPCC dataset and the different configurations of the two models. (a) GPCC (black line), CNRM-CM3 (blue line) and CNRM-CM5 (red line). (b) same as (a), but for IPSL-CM3 (blue line) and IPSL-CM5 (red line). On each panel, the thick red line and red shading show, respectively, the ensemble-mean standard-deviation and the spread among the individual members of the historical simulations for the CMIP5 version of the models.

Figure 10: Power spectra of detrended JJAS Indian rainfall time series estimated from the observations (GPCC) and the different simulations. (a) GPCC (black line), CNRM-CM3 (blue line), CNRM-CM5 individual simulations (red line) and CNRM-CM5 ensemble-mean spectrum (green line). (b) Same as (a), but for IPSL-CM3 and IPSL-CM5. The bottom axis of each panel is the period (unit: month), the left axis is variance (unit: $(mm/day)^2$) and both axes are in logarithm scale. The power spectrum is estimated using a FFT algorithm on overlapping segments (Welch, 1967) and the point-wise 99% confidence interval for the spectrum estimated from the observations is plotted in black dashed lines in each panel.

Figure 11: (a) Lead-lag correlations between ISM rainfall and monthly Niño-3.4 SSTs for observations (black line), CNRM-CM3 (blue line), and CNRM-CM5 (red line)

configurations, starting from the beginning of the previous year (e.g. year -1) to the end of the following year of the monsoon (e.g. year +1). GPCP rainfall and HadISST datasets are used for the observations and the period 1900-2000 are used to estimate the correlation coefficients in all cases. X-axis indicates calendar month for a 36 months period starting one year before the developing year of ISM and Y-axis is the amplitude of the correlation. The dashed lines indicate the 99% significance level according to a two-tailed student t-test. (b) Same as (a), but for IPSL-CM3 and IPSL-CM5. (c) Lead-lag correlations between the ISM dynamical index and monthly Niño-3.4 SSTs for the observations (black line), CNRM-CM3 (blue line) and CNRM-CM5 (red line); ERA40 and HadISST datasets are used for the observations. (d), Same as (c), but for IPSL-CM3 and IPSL-CM5.

Figure 12: (a) Lead and lag correlations between bi-monthly averaged Indo-Pacific SSTs and ISM rainfall estimated from the GPCC and HadISST datasets for the period 1900-2000. The correlations are calculated beginning in February-March, prior to the ISM, and ending in December-January after ISM. Correlations that are above the 90% significance confidence level according to a phase-scramble bootstrap test (Ebisuzaki, 1997) are underlined. (b) Same as (a), but for CNRM-CM5. (c) Same as (a), but for IPSL-CM5. In (b) and (c), the ensemble-mean correlation patterns and critical probabilities are plotted.

Figure 13: (a) 21-years sliding correlations between ISM rainfall and boreal summer (JJAS) Niño-3.4 SST time series in observations (black line; GPCC and HadISST datasets are used) and CNRM-CM5. The thick red line and red shading show, respectively, the ensemble-mean sliding correlations and the spread among the individual members of the historical simulations for CNRM-CM5. (b) Same as (a), but for IPSL-CM5. The thick red line and the thin red lines show, respectively, the ensemble-mean sliding correlations and the spread among the individual members of the historical simulations for IPSL-CM5

Figure 1

Past evolution of Indian summer rainfall (June to September)
observations and IPCC-AR4 simulations (20C3M)

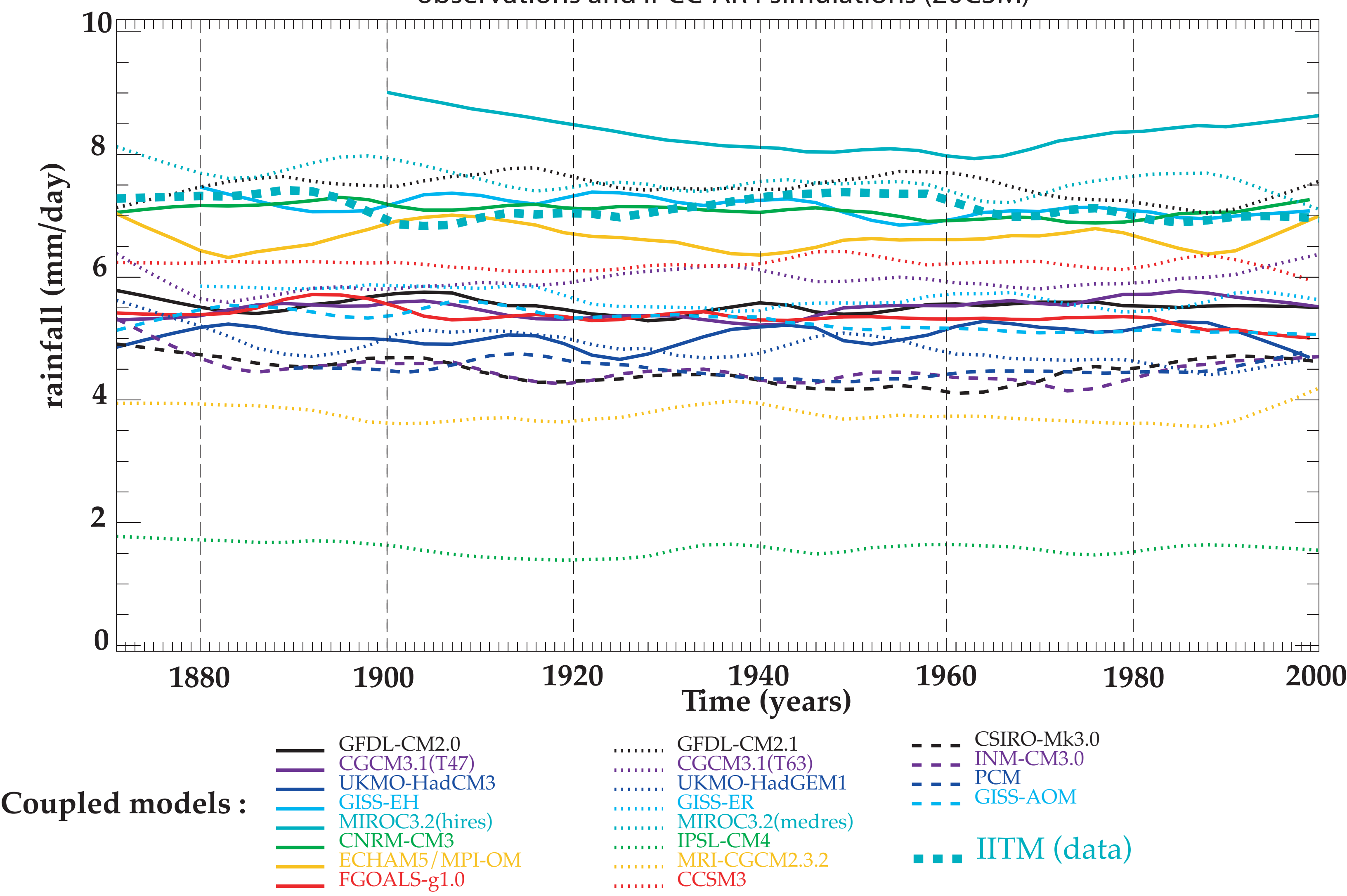

Figure 2

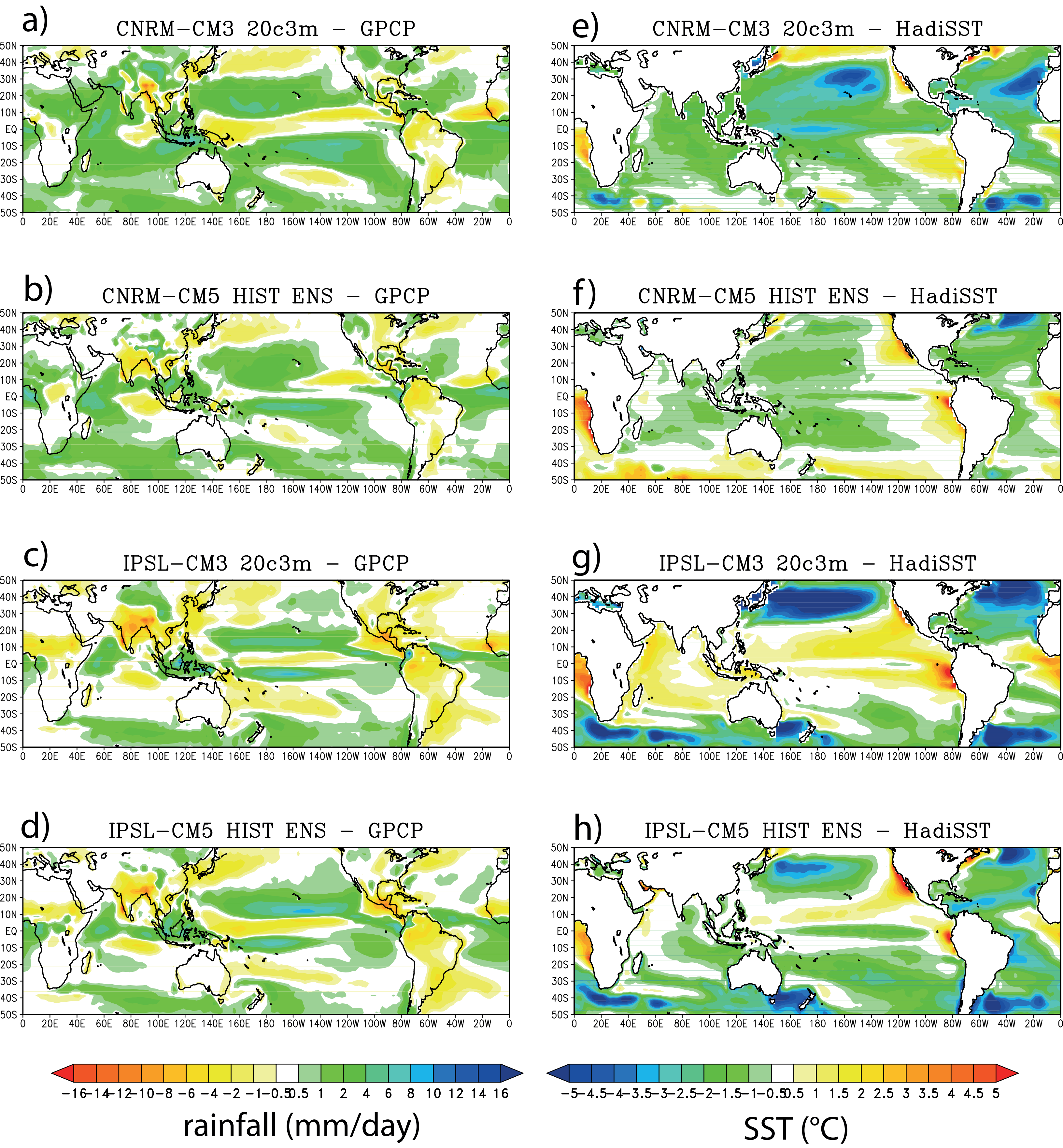
a) CNRM-CM3 20c3m - GPCP
b) CNRM-CM5 HIST ENS - GPCP
c) IPSL-CM3 20c3m - GPCP
d) IPSL-CM5 HIST ENS - GPCP
e) CNRM-CM3 20c3m - HadiSST
f) CNRM-CM5 HIST ENS - HadiSST
g) IPSL-CM3 20c3m - HadiSST
h) IPSL-CM5 HIST ENS - HadiSST
rainfall (mm/day)
SST (°C)

Figure 3

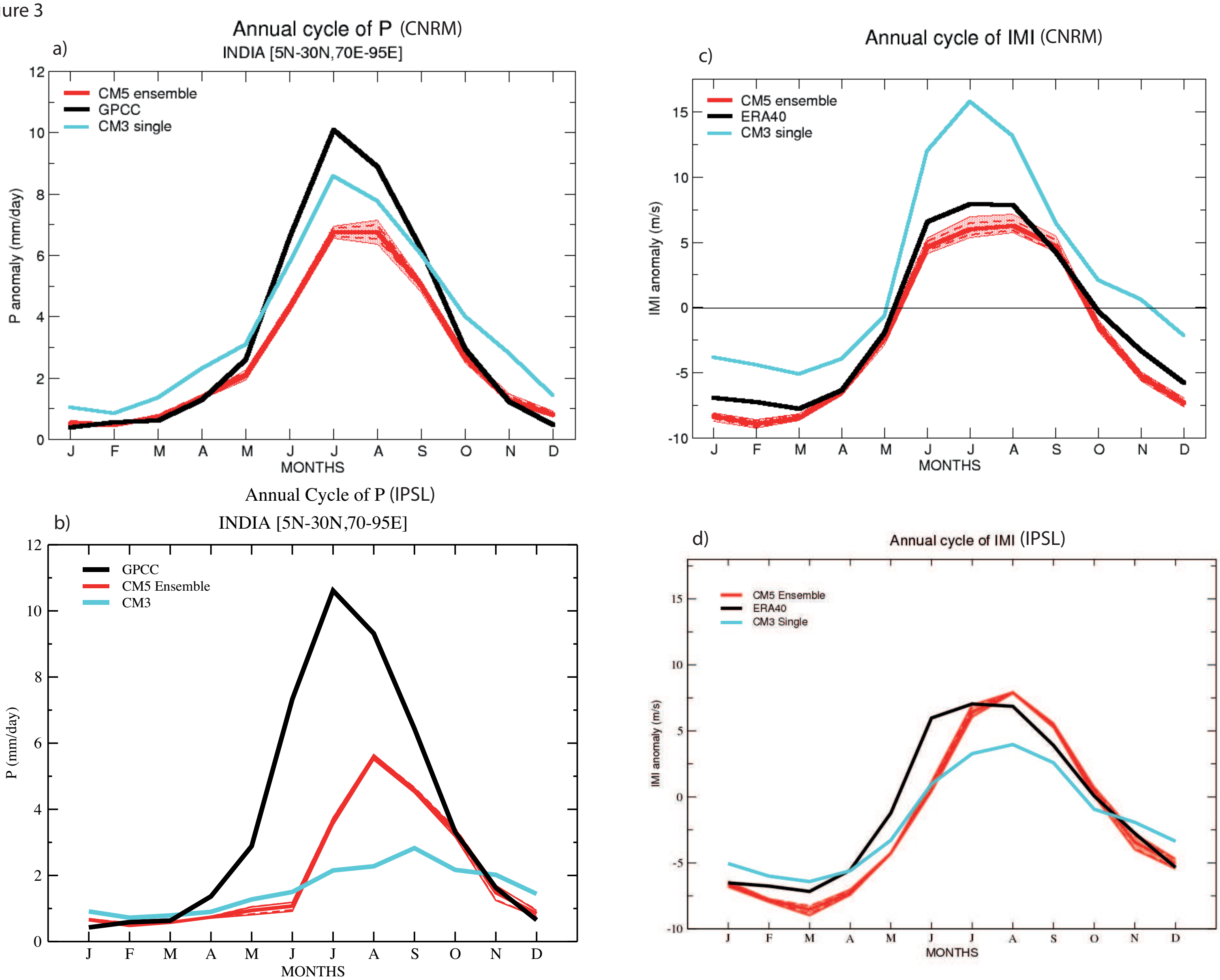

Annual cycle of P (CNRM)
a)
INDIA [5N-30N,70E-95E]
CM5 ensemble
GPCC
CM3 single
P anomaly (mm/day)
MONTHS
J F M A M J J A S O N D
Annual cycle of IMI (CNRM)
c)
CM5 ensemble
ERA40
CM3 single
IMI anomaly (m/s)
MONTHS
Annual Cycle of P (IPSL)
b)
INDIA [5N-30N,70-95E]
GPCC
CM5 Ensemble
CM3
P (mm/day)
MONTHS
d)
Annual cycle of IMI (IPSL)
CM5 Ensemble
ERA40
CM3 Single
IMI anomaly (m/s)
MONTHS

Figure 4

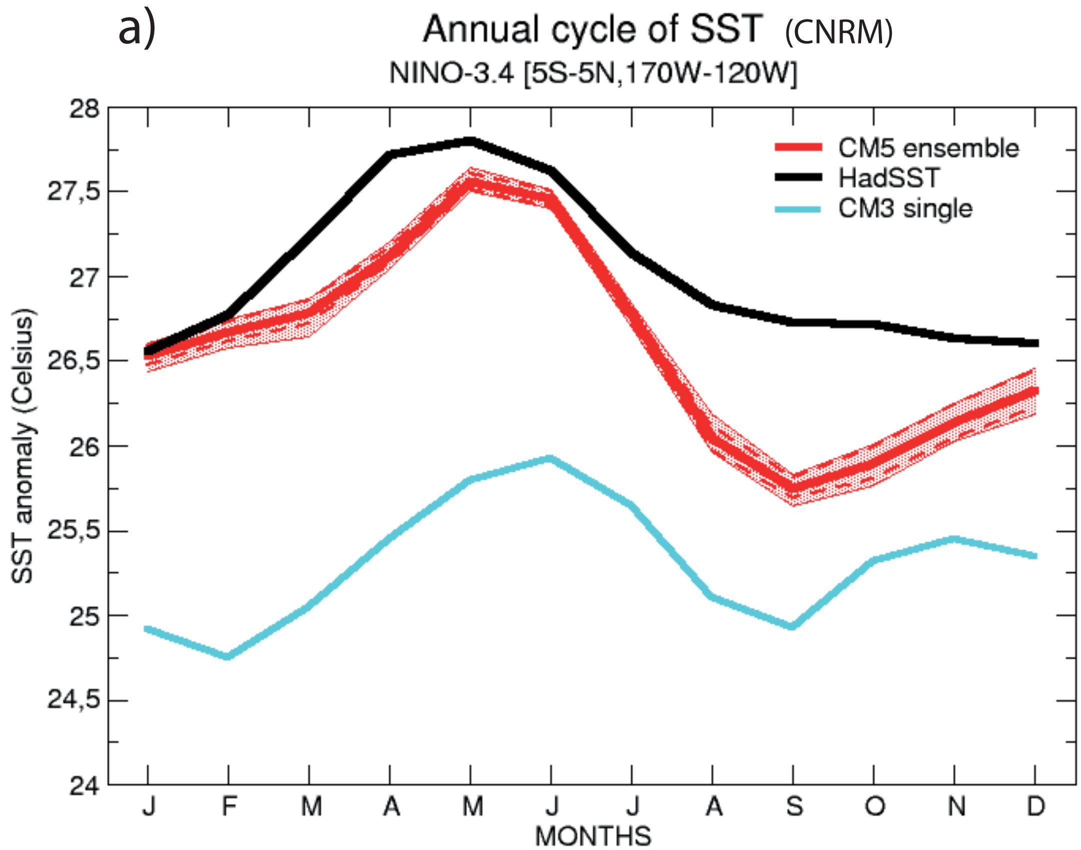

a)
Annual cycle of SST (CNRM)
NINO-3.4 [5S-5N,170W-120W]
CM5 ensemble
HadSST
CM3 single
SST anomaly (Celsius)
28
27,5
27
26,5
26
25,5
25
24,5
24
J
F
M
A
M
J
J
A
S
O
N
D
MONTHS

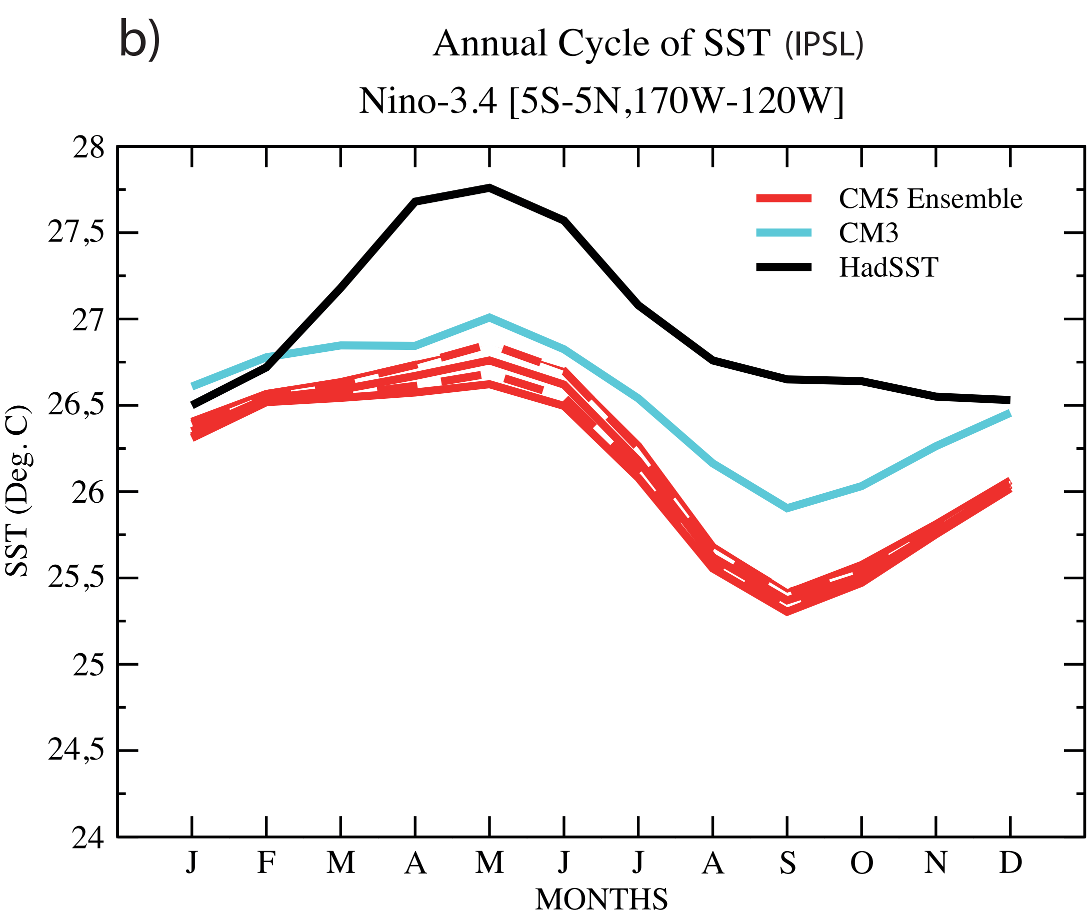

b)
Annual Cycle of SST (IPSL)
Nino-3.4 [5S-5N,170W-120W]
CM5 Ensemble
CM3
HadSST
SST (Deg. C)
28
27,5
27
26,5
26
25,5
25
24,5
24
J
F
M
A
M
J
J
A
S
O
N
D
MONTHS

Figure 5

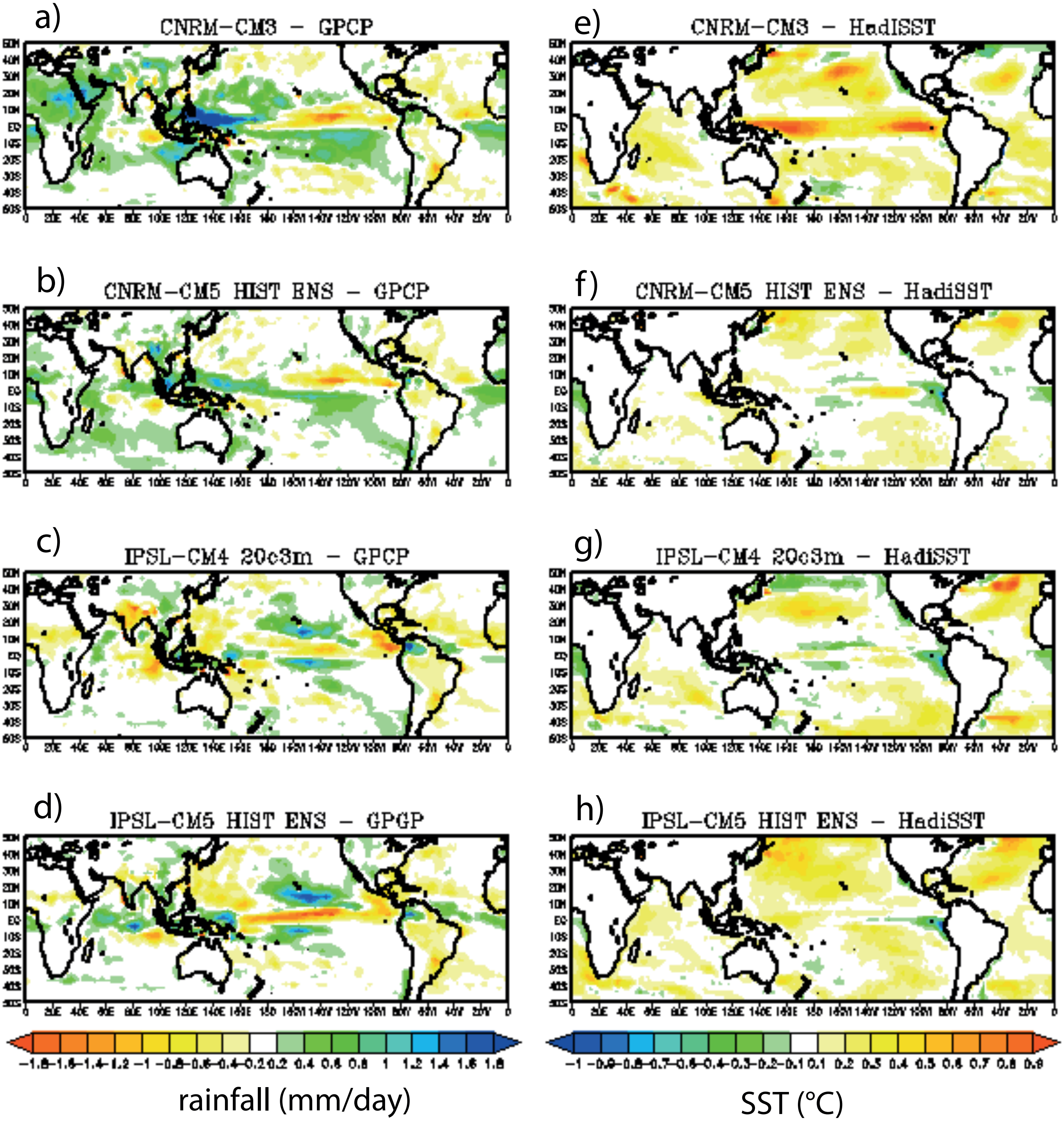
a)
CNRM-CM3 - GPCP
b)
CNRM-CM5 HIST ENS - GPCP
c)
IPSL-CM4 20c3m - GPCP
d)
IPSL-CM5 HIST ENS - GPGP
e)
CNRM-CM3 - HadISST
f)
CNRM-CM5 HIST ENS - HadISST
g)
IPSL-CM4 20c3m - HadISST
h)
IPSL-CM5 HIST ENS - HadiSST
rainfall (mm/day)
SST (°C)

Figure 6

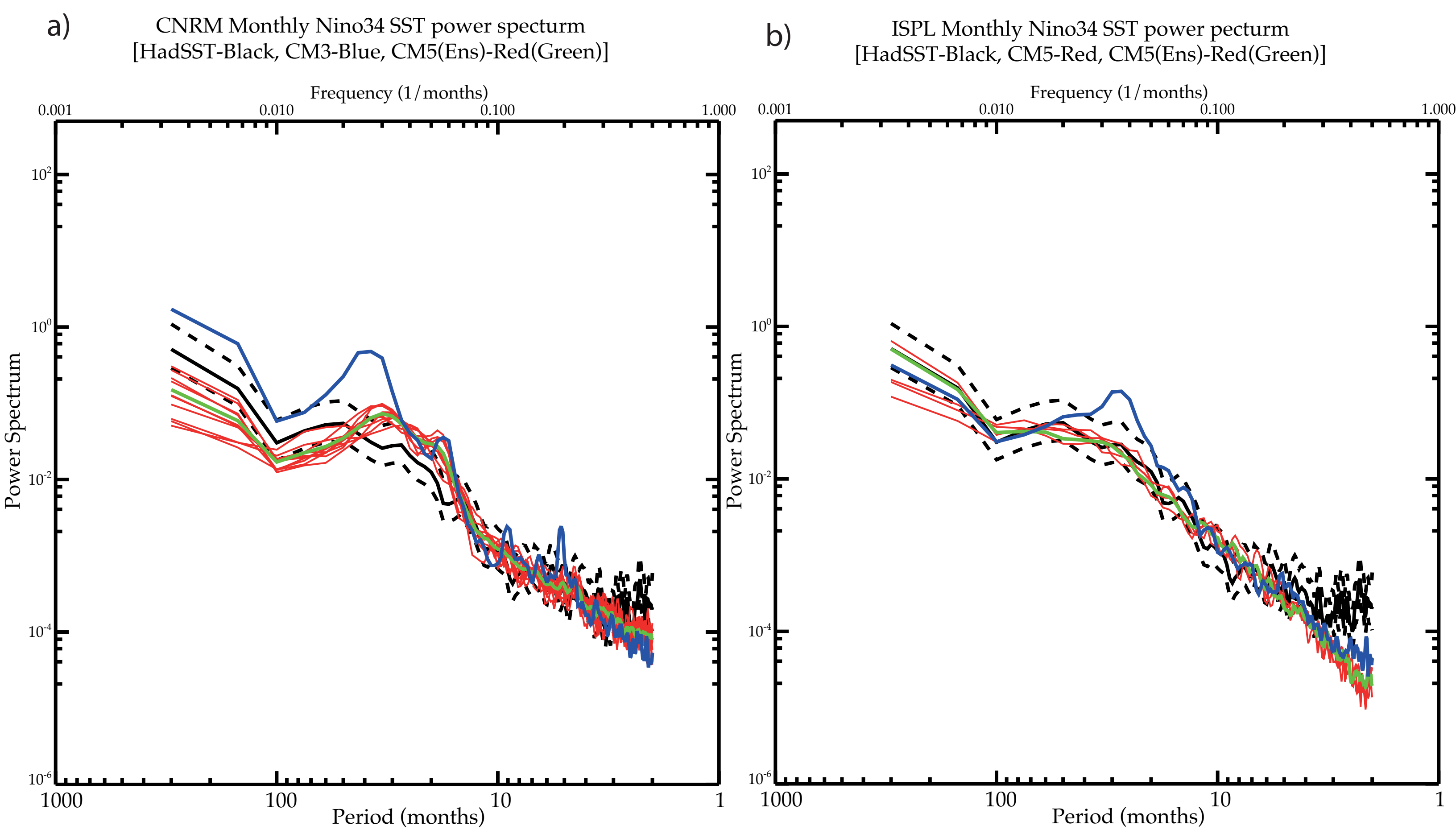

a)
CNRM Monthly Nino34 SST power specturm
[HadSST-Black, CM3-Blue, CM5(Ens)-Red(Green)]
Frequency (1/months)
0.001
0.010
0.100
1.000
Power Spectrum
10^{2}
10^{0}
10^{-2}
10^{-4}
10^{-6}
1000
100
10
1
Period (months)
b)
ISPL Monthly Nino34 SST power pecturm
[HadSST-Black, CM5-Red, CM5(Ens)-Red(Green)]
Frequency (1/months)
0.001
0.010
0.100
1.000
Power Spectrum
10^{2}
10^{0}
10^{-2}
10^{-4}
10^{-6}
1000
100
10
1
Period (months)

Figure 7

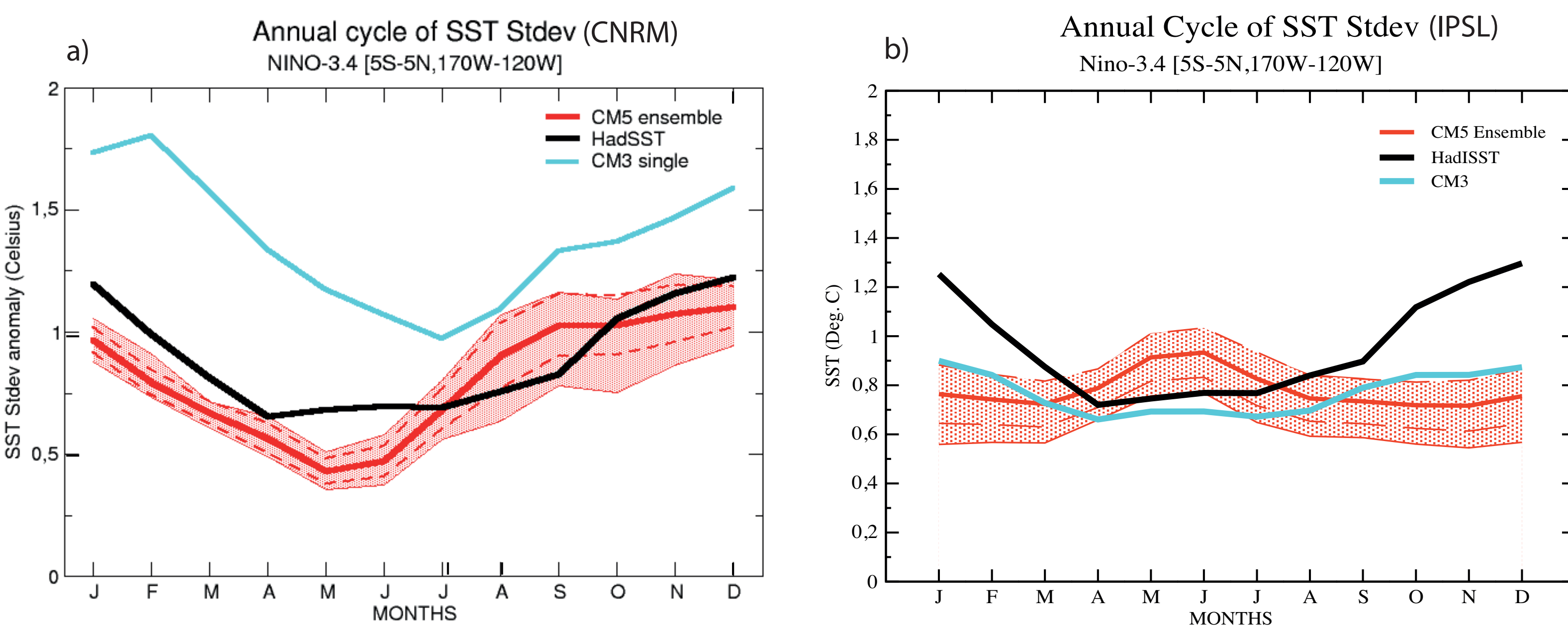
a)
Annual cycle of SST Stdev (CNRM)
NINO-3.4 [5S-5N,170W-120W]
SST Stdev anomaly (Celsius)
MONTHS
CM5 ensemble
HadSST
CM3 single
b)
Annual Cycle of SST Stdev (IPSL)
Nino-3.4 [5S-5N,170W-120W]
SST (Deg. C)
MONTHS
CM5 Ensemble
HadISST
CM3

Figure 8

a) Correlations between Detrended Bi-Monthly SST vs Nino34 DJF SST
HADISST (1901-2000)

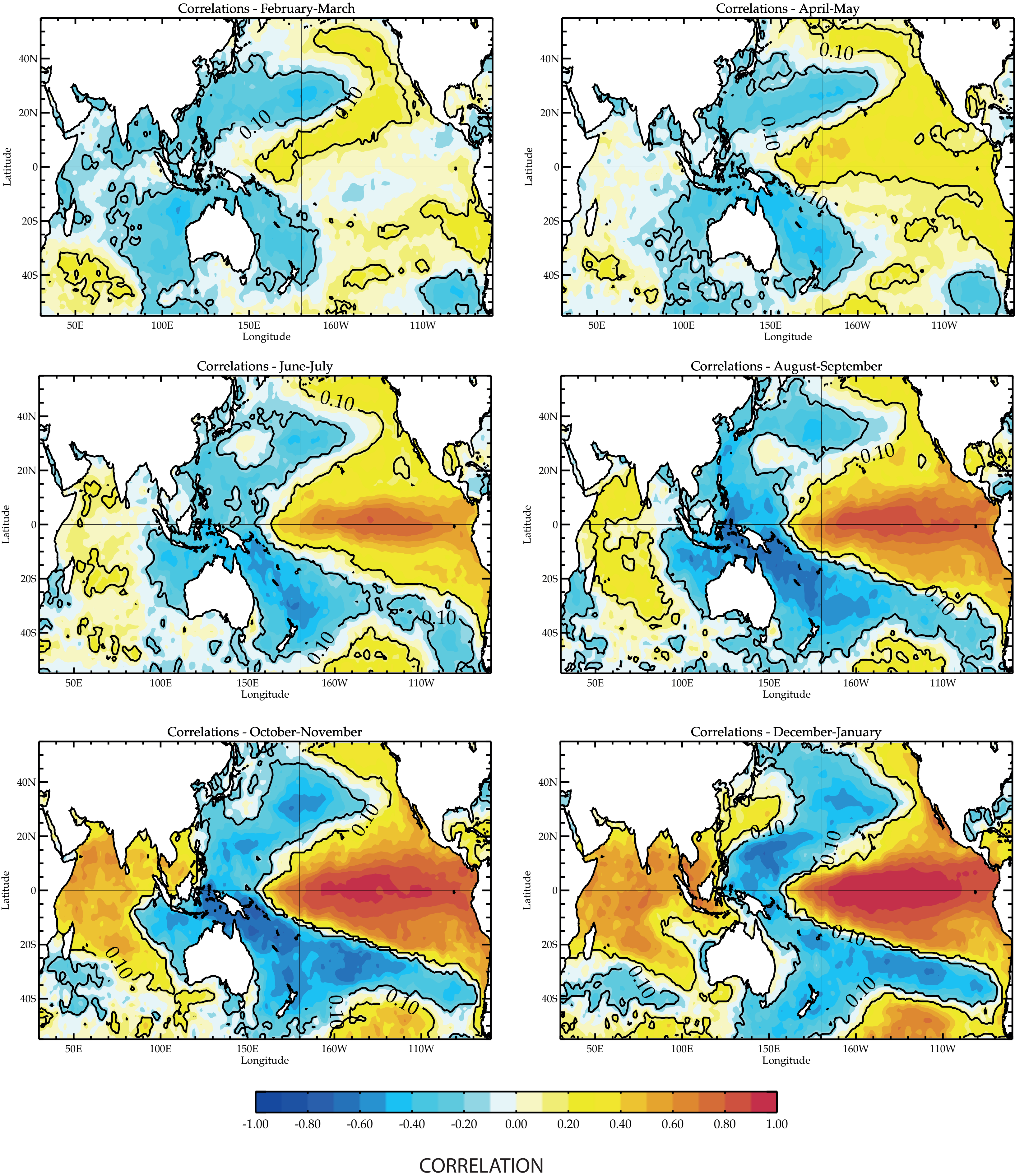

Figure 8

b) Correlations between Detrended Bi-Monthly SST vs Nino34 DJF SST CNRM HIST ENS (1901-2000)

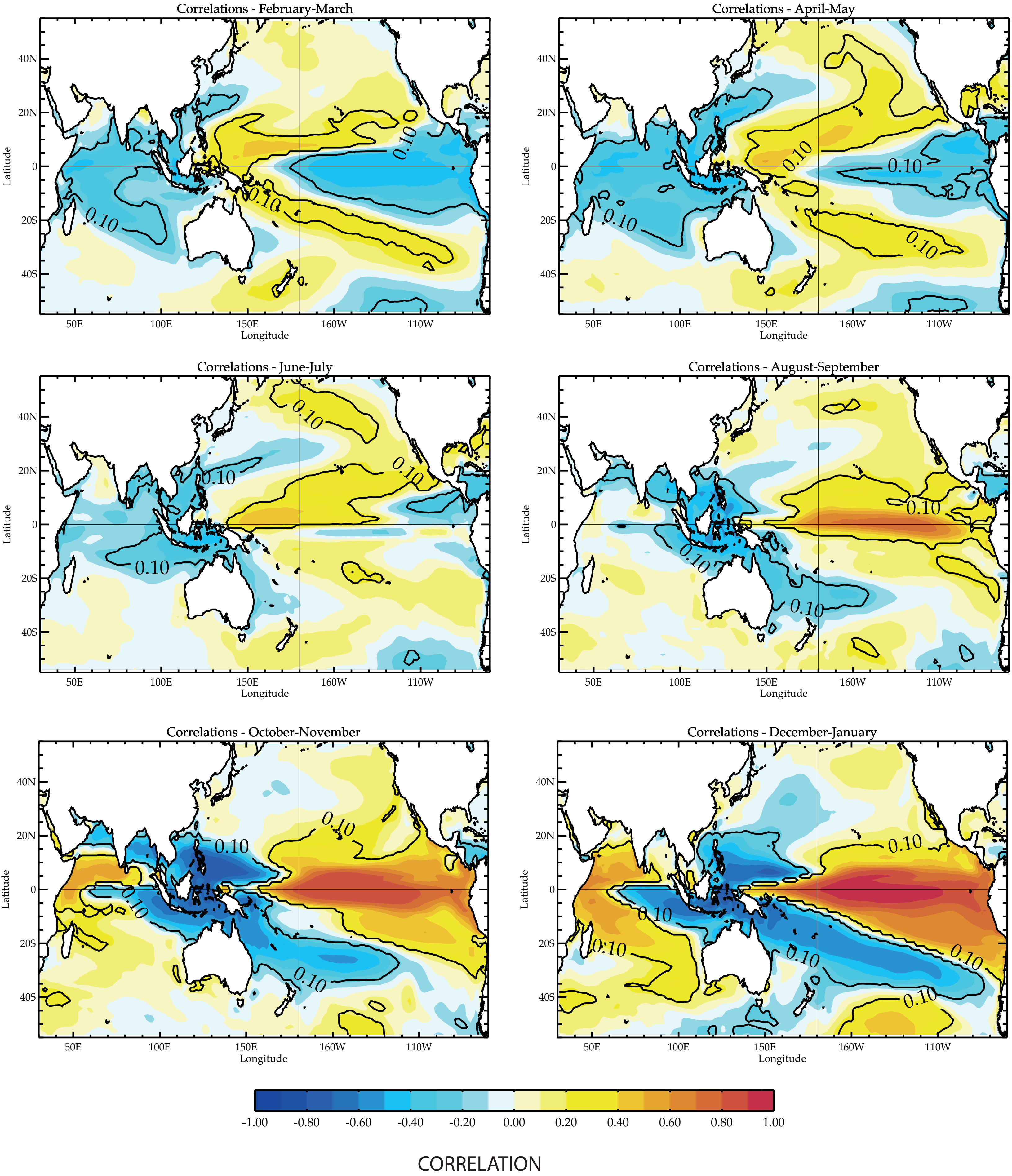

Figure 8

c) Correlations between Detrended Bi-Monthly SST vs Nino34 DJF SST
IPSL HIST ENS (1901-2000)

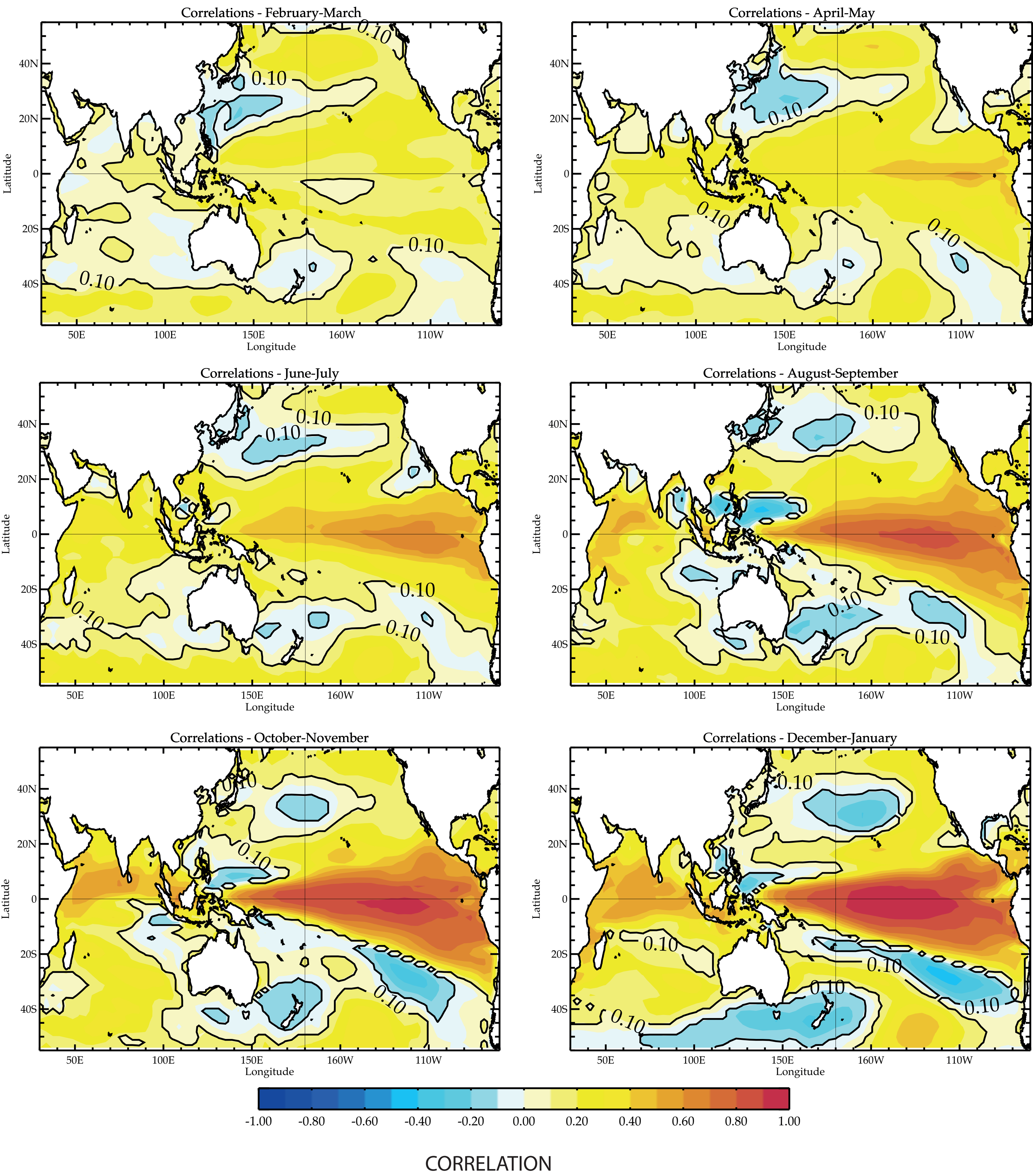

Figure 9

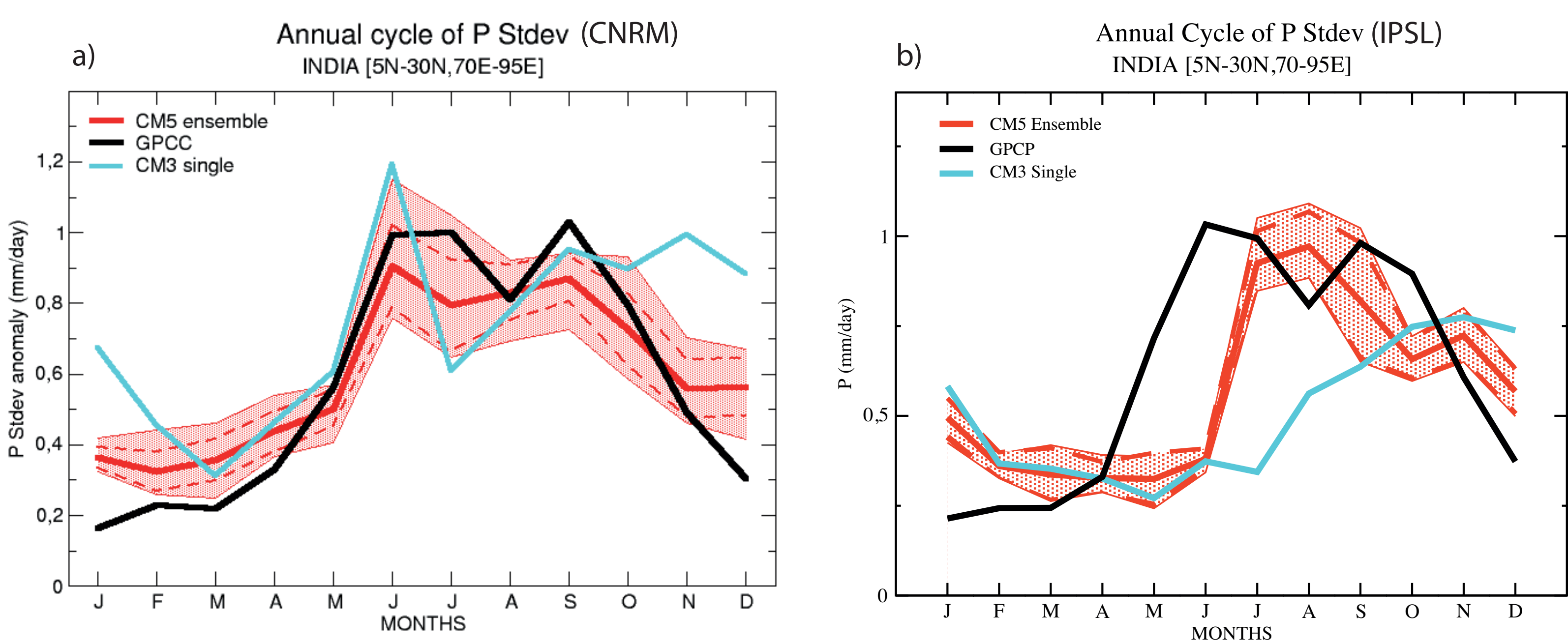
a)
Annual cycle of P Stdev (CNRM)
INDIA [5N-30N,70E-95E]
CM5 ensemble
GPCC
CM3 single
P Stdev anomaly (mm/day)
0
0,2
0,4
0,6
0,8
1
1,2
J F M A M J J A S O N D
MONTHS
b)
Annual Cycle of P Stdev (IPSL)
INDIA [5N-30N,70-95E]
CM5 Ensemble
GPCP
CM3 Single
P (mm/day)
0
0,5
1
J F M A M J J A S O N D
MONTHS

Figure 10

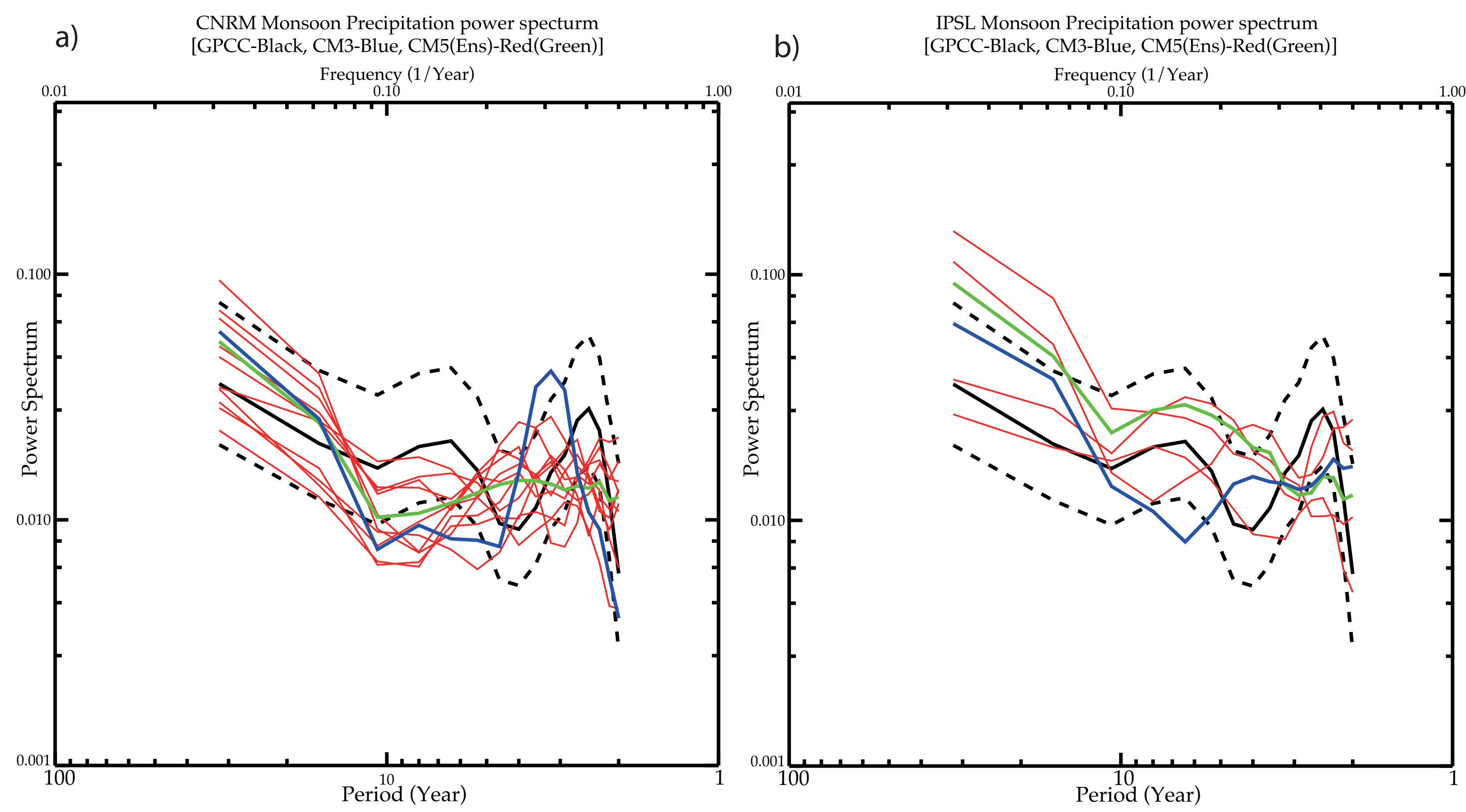
a)
CNRM Monsoon Precipitation power specturm
[GPCC-Black, CM3-Blue, CM5(Ens)-Red(Green)]
Frequency (1/Year)
0.01
0.10
1.00
Power Spectrum
0.100
0.010
0.001
100
10
1
Period (Year)
b)
IPSL Monsoon Precipitation power spectrum
[GPCC-Black, CM3-Blue, CM5(Ens)-Red(Green)]
Frequency (1/Year)
0.01
0.10
1.00
Power Spectrum
0.100
0.010
0.001
100
10
1
Period (Year)

Figure 11

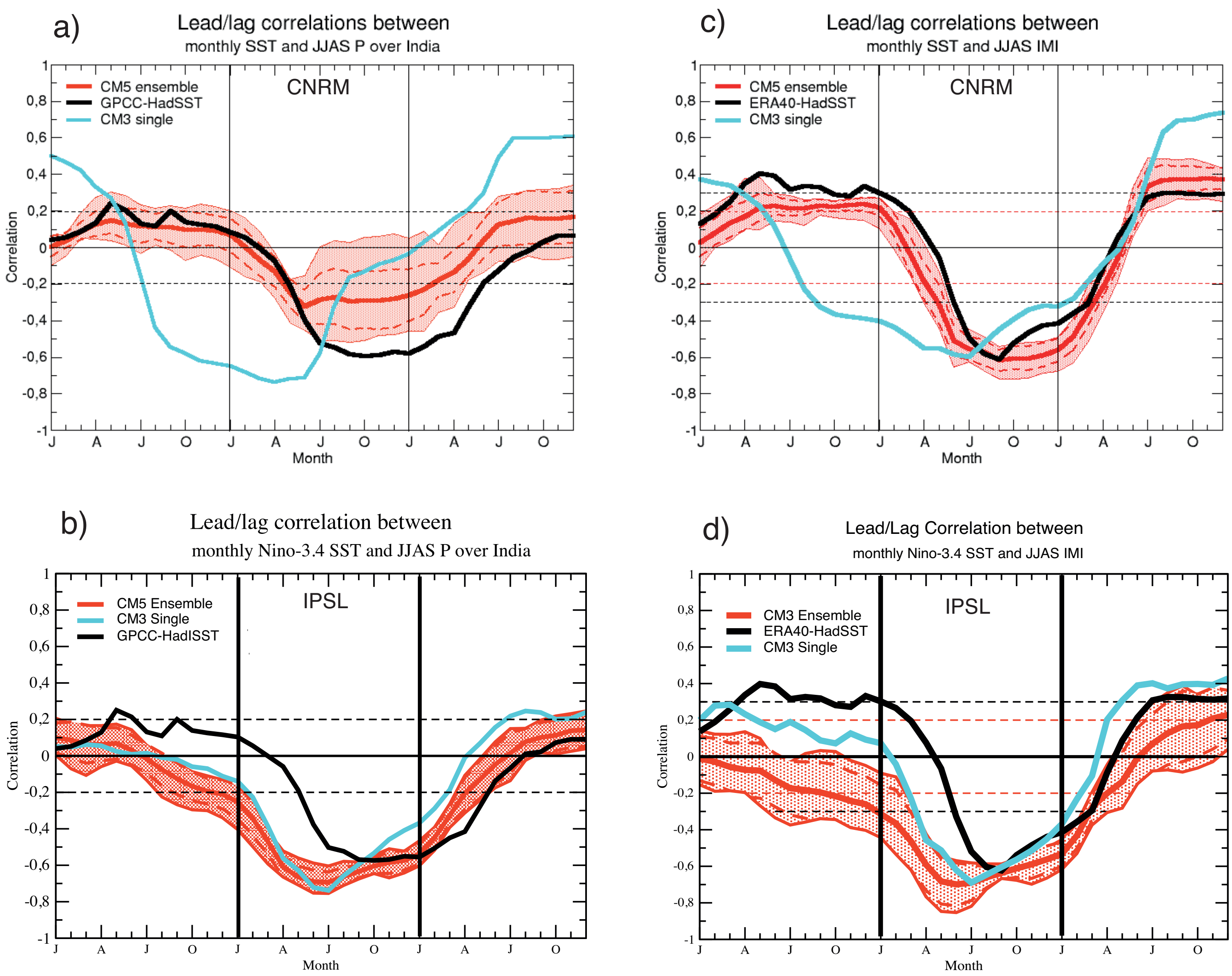
a)
Lead/lag correlations between
monthly SST and JJAS P over India
CNRM
CM5 ensemble
GPCC-HadSST
CM3 single
Correlation
Month
b)
Lead/lag correlation between
monthly Nino-3.4 SST and JJAS P over India
IPSL
CM5 Ensemble
CM3 Single
GPCC-HadISST
Correlation
Month
c)
Lead/lag correlations between
monthly SST and JJAS IMI
CNRM
CM5 ensemble
ERA40-HadSST
CM3 single
Correlation
Month
d)
Lead/Lag Correlation between
monthly Nino-3.4 SST and JJAS IMI
IPSL
CM3 Ensemble
ERA40-HadSST
CM3 Single
Correlation
Month

Figure 12

a) Correlations between Detrended Bi-Monthly SST vs JJAS Precip over India
HADISST and GPCC (1901-2000)

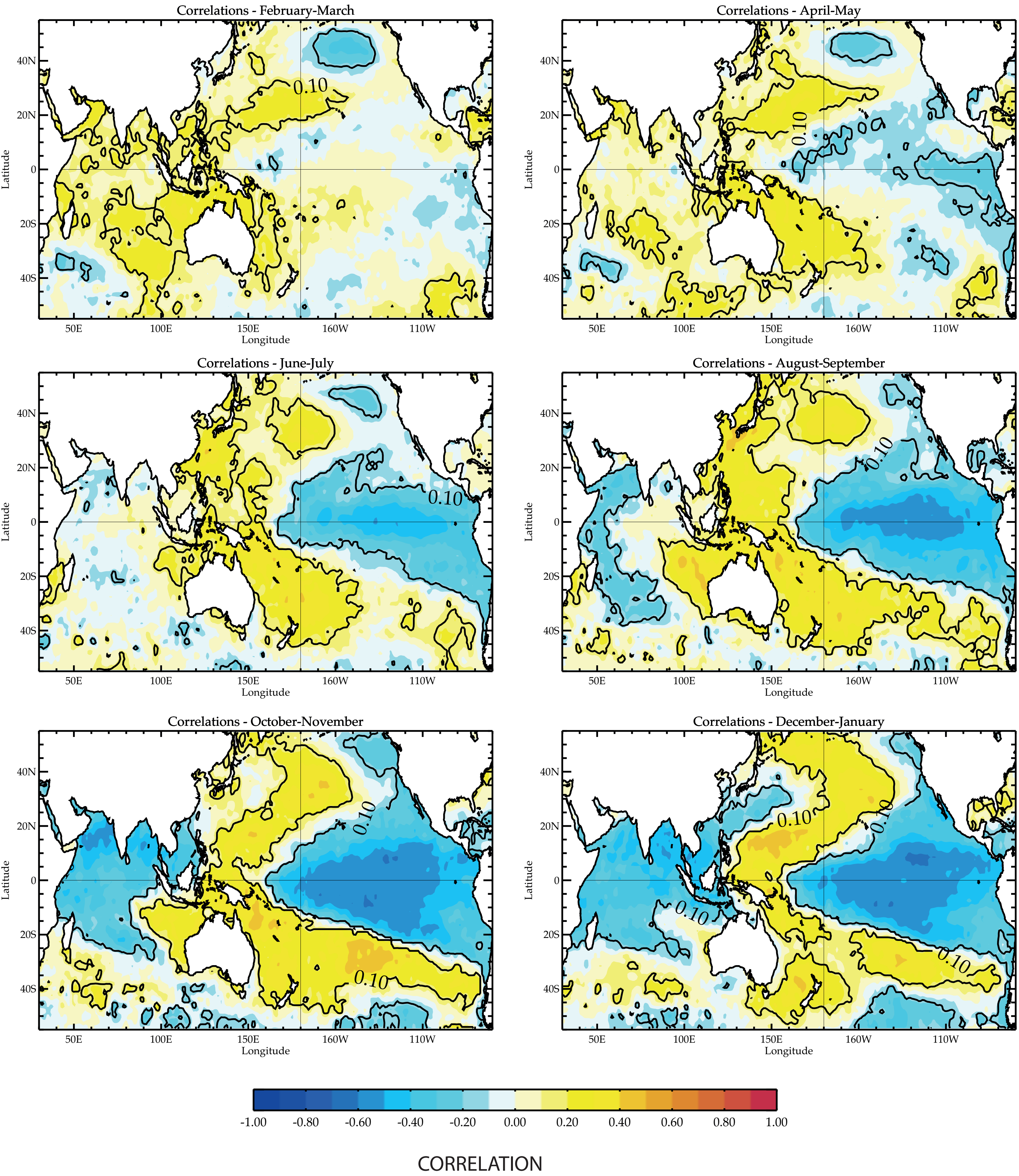

Figure12

b) Correlations between Detrended Bi-Monthly SST vs JJAS Precip over India
CNRM HIST ENS (1901-2000)

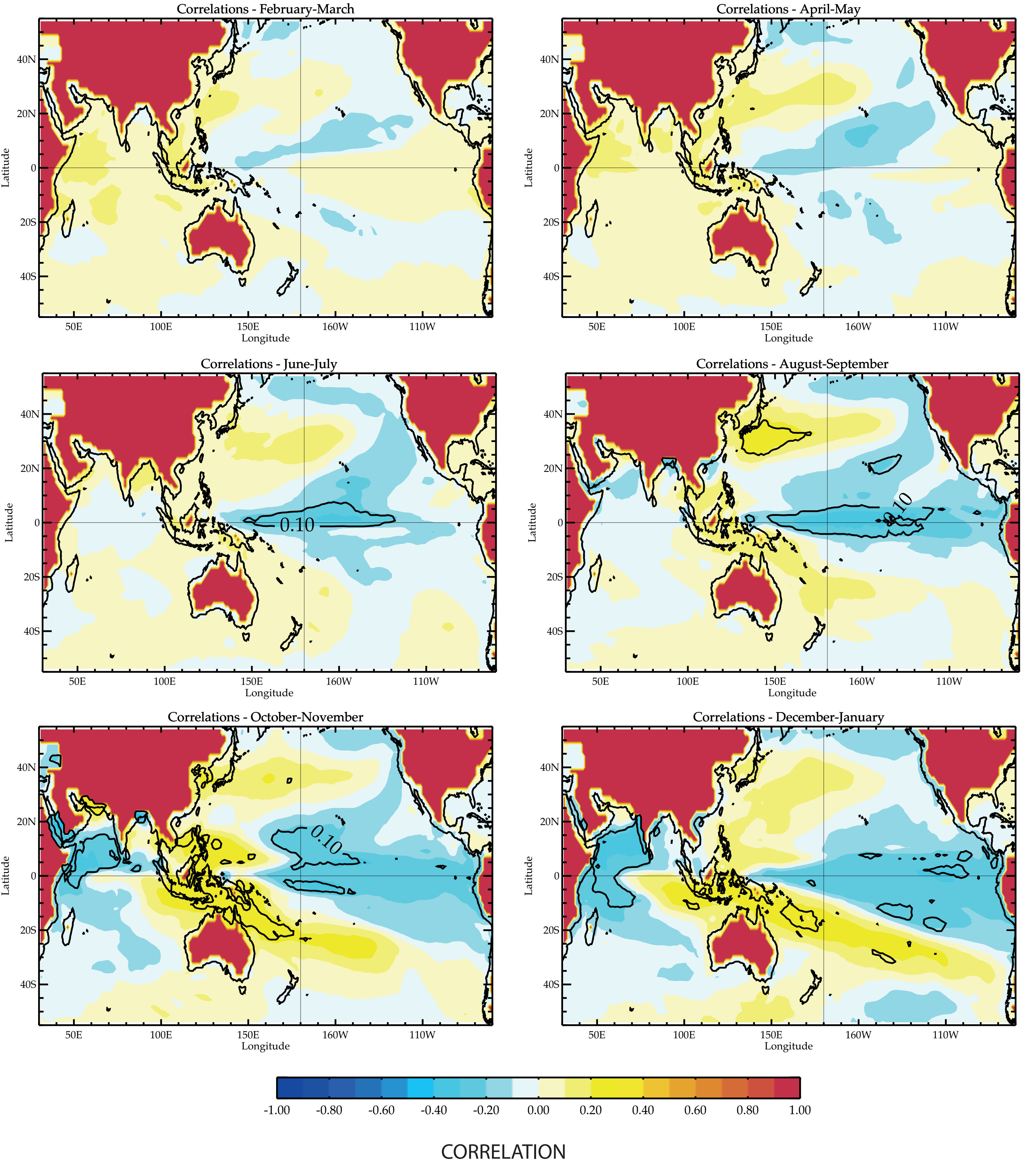

Figure 12

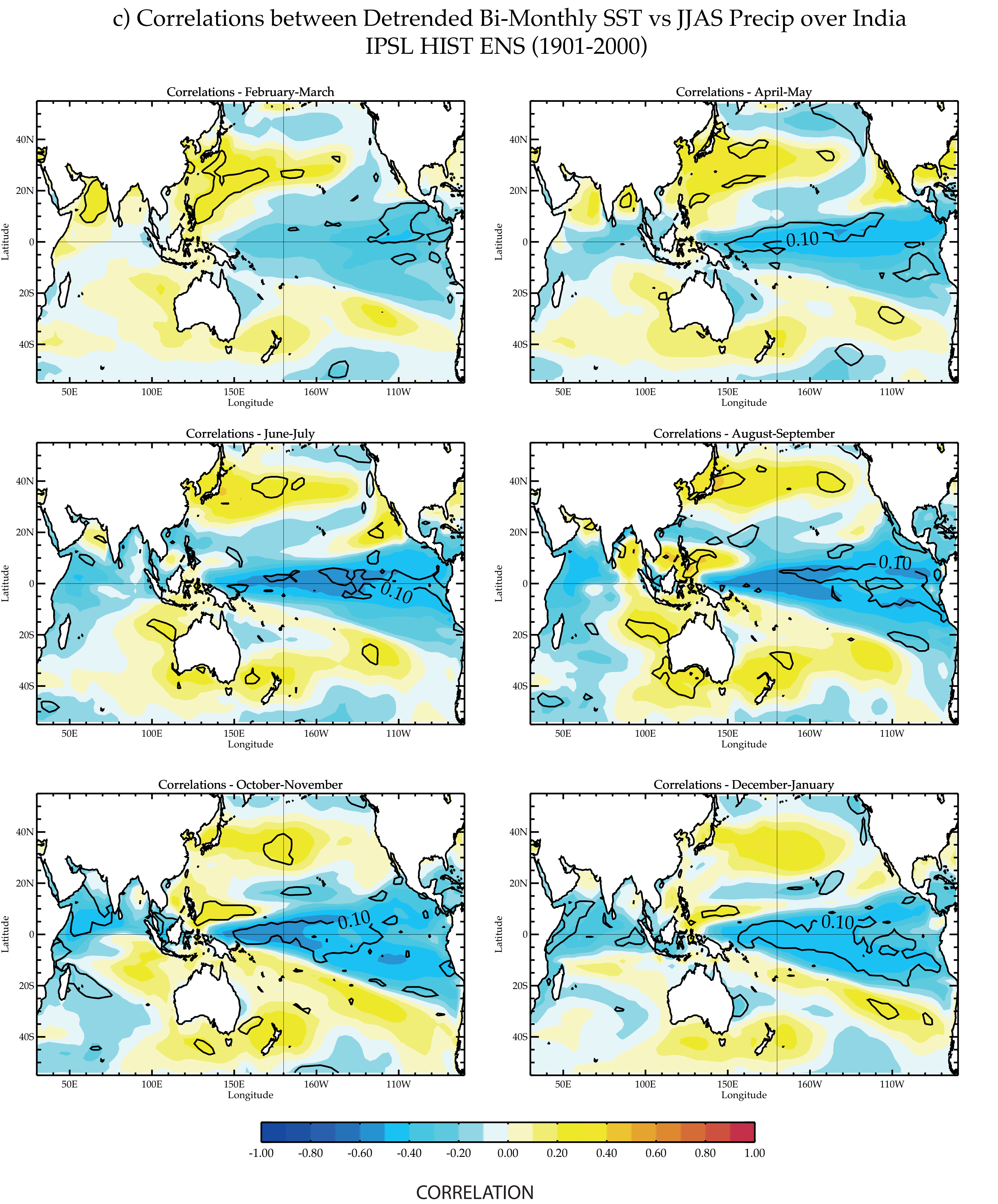

c) Correlations between Detrended Bi-Monthly SST vs JJAS Precip over India
IPSL HIST ENS (1901-2000)
Correlations - February-March
Correlations - April-May
Correlations - June-July
Correlations - August-September
Correlations - October-November
Correlations - December-January
0.10
40N
20N
0
20S
40S
Latitude
50E
100E
150E
160W
110W
Longitude
-1.00
-0.80
-0.60
-0.40
-0.20
0.00
0.20
0.40
0.60
0.80
1.00
CORRELATION

Figure 13

a)

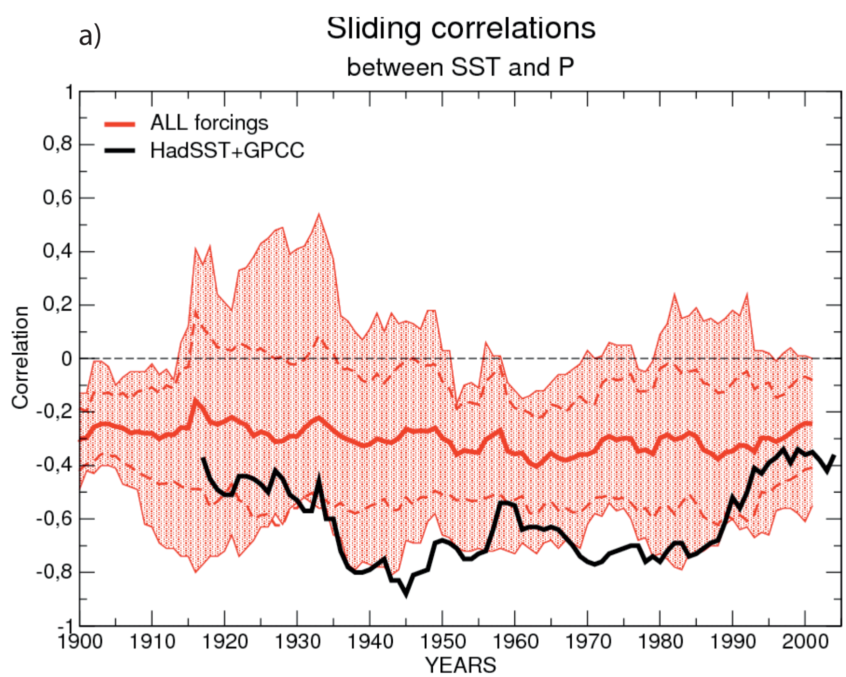
Sliding correlations
between SST and P
ALL forcings
HadSST+GPCC
Correlation
1
0,8
0,6
0,4
0,2
0
-0,2
-0,4
-0,6
-0,8
-1
1900
1910
1920
1930
1940
1950
1960
1970
1980
1990
2000
YEARS

b)

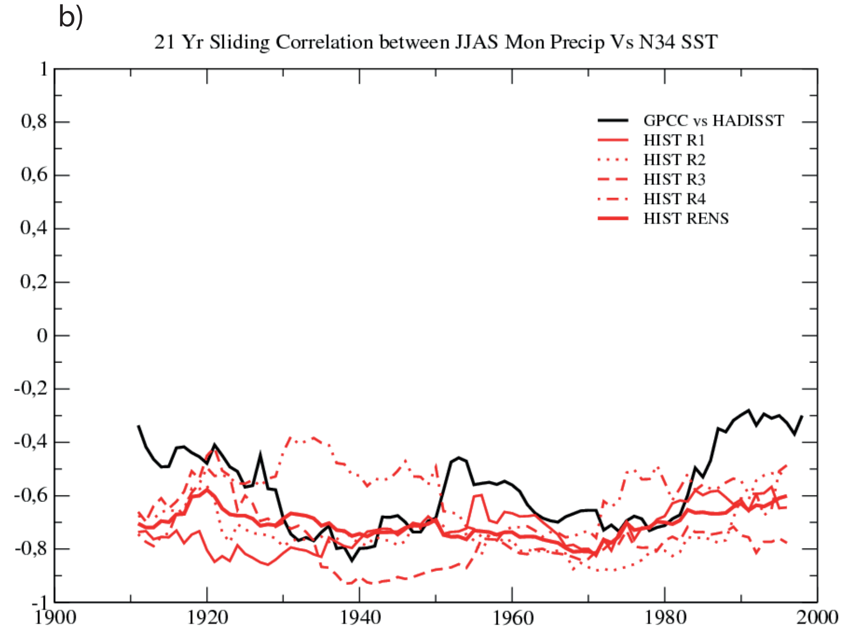
21 Yr Sliding Correlation between JJAS Mon Precip Vs N34 SST
GPCC vs HADISST
HIST R1
HIST R2
HIST R3
HIST R4
HIST RENS
1
0,8
0,6
0,4
0,2
0
-0,2
-0,4
-0,6
-0,8
-1
1900
1920
1940
1960
1980
2000